

Extracting Cosmological Parameters from Cosmic Microwave Background
Temperature Map Data

A Thesis
Presented to
The Division of Mathematics and Natural Sciences
Reed College

In Partial Fulfillment
of the Requirements for the Degree
Bachelor of Arts

Samuel F. Coscia

May 2024

Approved for the Division
(Physics)

Alison Crocker

Acknowledgements

There are so many people to thank for supporting me and helping me get through Reed and life in general.

First, I want to thank the professors I have had at Reed that have been so inspiring. This is Joel Franklin, Noah Charles, Alison Crocker, Johnny Powell, and Owen Gross. You all have been wonderful mentors and have always been willing to help me when I am struggling. Owen, thank you for such a wonderful experience working as a lab 101/102 TA. It is truly something I will never forget, and has been one of the most fun jobs I have ever had.

Jim Napolitano and the Napolitano lab group: You are all wonderful people and I had the best time working with you all on the MOLLER polarimeter experiment over the summer of '23.

Michael LoStracco: you have always inspired me to think deeply about the world around me, and I will never forget our philosophical discussions.

Steve Heitzer, Dave Nolan, Mike Gamble, and Noah Simpson: You guys are the best music teachers someone could ask for and I am so grateful for the times we have gotten to work on music together.

Emma Perry and the Perry family: Thank you for always providing a home away from home (even though it was right across the street). Emma you have been a great friend to have grown up with, and you and your family have always been such a support.

To my friends in the physics department: Marc MacNamee, Anatalya Piatigorsky, Hope Palmer, Vivian Chen, and Alles. We did it! I am very happy to be graduating with all of you, and each of you are so wonderful and bright in your own way.

Milo Gardener-Stephens: You are such a great friend and I know I will always know you. Thank you so much for your support!

Gecko and Spider: I've never quite met cats like you guys, so wonderful and elegant. I'm always delighted to see you both on Sundays and share cuddles and love!

Table of Contents

Introduction	1
0.1 The Origins of the CMB	1
Chapter 1: Inflation, Anisotropy, and the CMB Power Spectrum	5
1.1 Determining the Power Spectrum	8
1.2 Contributions to Anisotropy	11
1.3 Methods of Calculation	19
1.4 Error Estimation	20
Chapter 2: Parameter Determination	25
2.1 Density Parameters	26
2.1.1 Baryon Density, Ω_B	29
2.1.2 Dark Matter Density, Ω_c	32
2.2 Summed Neutrino Mass, m_ν	33
2.3 Hubble Constant, H_0	35
2.4 Curvature Parameter, Ω_k	37
2.5 Reionization Optical Depth, τ	38
2.6 Consistency with Planck Parameters	40
Chapter 3: CosmoMC and Extensions	43
References	47

Abstract

Remnants of the Big Bang, the initial expansion of the universe, are accessible as leftover radiation from as early as 380,000 years into the history of the universe. This leftover radiation is called the cosmic microwave background (CMB), and is remarkably isotropic in accordance with Einstein's cosmological principle. Nevertheless, the CMB contains slight anisotropies in temperature variation around the sky (on the order of $\Delta T = 10^{-5}$ K), which is one of the primary pieces of evidence we have for cosmic inflation in the first fractions of a second of the universe. From these anisotropies, parameters necessary to describe the evolution of our universe in the Λ CDM model can be measured, and extracted using an angular power spectrum. For this thesis, I will explore the methods through which the following parameters are calculated: Ω_b , Ω_c , m_ν , H_0 , Ω_k and τ . Further, I will present our results from Planck satellite CMB measurements, showing what parameter values are consistent with our methods.

Dedication

My family: Addy, Gracie, Ella, Eli, Aidan, Patrick, Corinne, and especially my mom and dad, Tricia and Joe Coscia. You have all greatly helped me get to where I am now in my study of physics and I am forever grateful for your support and love. I would not be where I am now without any one of you.

Edy Sarceno: Man, I don't even need to say anything, you already know, but your constant love and support has kept me going even through the worst of times and I would not be the same without you. You are truly a brother to me.

Hannah Chubin: Spending time with you this past year has made me such a better person, and you are a wonderful partner that I will be forever grateful for.

Chris Odom: Taking your AP physics class and robotics classes were some of the most meaningful experiences I have had in academia. I will always be grateful for the way you taught physics, inspiring me to push forward to the point I am now.

Uncle Jimmy (Dr. James Crawford): I will never forget our summer spent together learning special relativity, and the many conversations we have had about physics. You inspired me to continue my path as a physicist and I truly look up to you in so many ways for that. It is so wonderful that there is another physicist in the family that I can share all my thoughts with.

Alison Crocker: I have never talked to you about this, but in high school when I was still deciding where to go to college, I was interested in Reed but not fully dedicated to it as my top choice. My dad then showed me a video about you winning an award for teaching astrophysics, and I was sold, you seemed like an amazing teacher and someone I really wanted to work with, especially in a smaller school environment to learn astrophysics and cosmology. I am so glad to have done this thesis with you, and it has turned out wonderfully. Thank you for inspiring me to come to Reed.

Quark: You are the most wonderful dog I could ask for, and truly my partner in crime wherever I go. I love you so much and you have taught me so much about cosmology and physics!

Introduction

Then God said, “Let there be light”; and there was light. (Genesis 1:3)

0.1 The Origins of the CMB

As far as we currently know, the early universe began with an extreme expansion of space from a highly dense state. This constitutes the “Big Bang” and is predicted by empirical evidence from Edwin Hubble suggesting that the universe is expanding, and by the standard model of cosmology (also called the Λ CDM model).¹ The Λ CDM model is cosmologists’ best current model of the large-scale universe thus far, resulting naturally from the mathematics of general relativity given a homogeneous and isotropic universe on large scales, and accounting for dark energy and dark matter.² As a result of the Big Bang theory, we expect an afterglow of radiation still visible from the early universe, but redshifted into the microwave wavelength regime. Remarkably, this cosmic microwave background has been measured (first in 1965 by physicists Penzias and Wilson from excess temperature noise detected by an antennae) and is in accordance with the standard model.³

According to predictions of the standard model, immediately after the Big Bang, the universe rapidly inflated which ended with its energy converting to matter, a “hot soup” of plasma consisting of baryons, electrons, radiation, dark matter and dark energy. When this conversion took place, the universe kept expanding, but cooled and expanded at a slower rate. Once the universe cooled enough, to around $2 * 10^{12}$ K, this is when the strong force allowed quarks to form protons and neutrons.⁴ Protons and neutrons later joined together to create the first atomic nuclei as we know it, mostly consisting of ionized hydrogen and helium, though other light elements such as lithium were also formed.⁵ At this time, free electrons were so abundant that light could not travel very far without interacting with them (in other words, light had a short mean free path).⁶

At around 380,000 years after the Big Bang, it is predicted by the standard model that the universe cooled enough so that electrons could bind to the ionized atomic

¹Schneider (2006)

²Schneider (2006)

³Penzias & Wilson (1965)

⁴Carroll & Ostlie (2014)

⁵Carroll & Ostlie (2014)

⁶Schneider (2006)

nuclei, forming the first atoms. The impact the formation of the first atoms had on the dynamics and distribution of photons at this time was that these photons then had a very significantly longer mean free path, which is to say that they could travel the universe largely unimpeded by interactions with electric charges. Essentially, the pattern of these photons around the sky was then ‘frozen’ in time, still detectable today with our measurement systems on Earth, such as satellites and antennae, and called the cosmic microwave background, or CMB.⁷ The CMB photons all come from a celestial sphere that is located at a redshift of around 1100, commonly denoted as the surface of last scattering.⁸

Built into the assumptions that imply a Big Bang is Einstein’s cosmological principle. Einstein’s cosmological principle states that the universe is close to both completely homogeneous (the same in all locations) and isotropic (the same in all directions) on the largest scales (scales greater than 250 million light years across). These assumptions have been in large agreement with observation, over numerous tests, including measurements of the CMB, which is very nearly isotropic. As several satellite measurements have now shown, there is slight temperature variation in this distribution of these photons, making the CMB slightly anisotropic.⁹ A map of these temperature anisotropies around the sky and projected into flat, 2 dimensional space (in what is called a Mollweide projection) can be seen in Figure 1. Satellite measurements of the CMB anisotropies include the COBE, WMAP, and Planck satellites, and have increased in resolution over time as can be seen by Figure 2. These anisotropies are very important, as they give rise to techniques (used in this thesis and in the standard model of cosmology) for determining six base independent cosmological parameters required for the standard model: the Hubble constant, H_0 , the baryon density of the universe, Ω_b , the cold dark matter density, Ω_c , the summed neutrino mass, m_ν , the curvature parameter, Ω_k , and the reionization optical depth, τ . In this thesis, the method for determining these parameters will be through finding an angular power spectrum of the Planck 2018 CMB temperature map. This angular power spectrum is highly dependent on the cosmological parameters, so it is useful for their estimation.

I will begin by expanding on necessary theoretical aspects of the cosmic microwave background, Big Bang cosmology, and the cosmological parameters in order to provide a more in-depth understanding of these topics. I will then describe the mathematical methods for calculating cosmological parameters from the CMB in detail, as well as show the results of my own calculations using the Planck 2018 data release. The primary method of obtaining parameter values will be through calculating the angular power spectrum of temperature fluctuations/anisotropies, using public sky-map data made available by the Planck collaboration.

⁷Schneider (2006)

⁸Callin (2006); Schneider (2006)

⁹Schneider (2006)

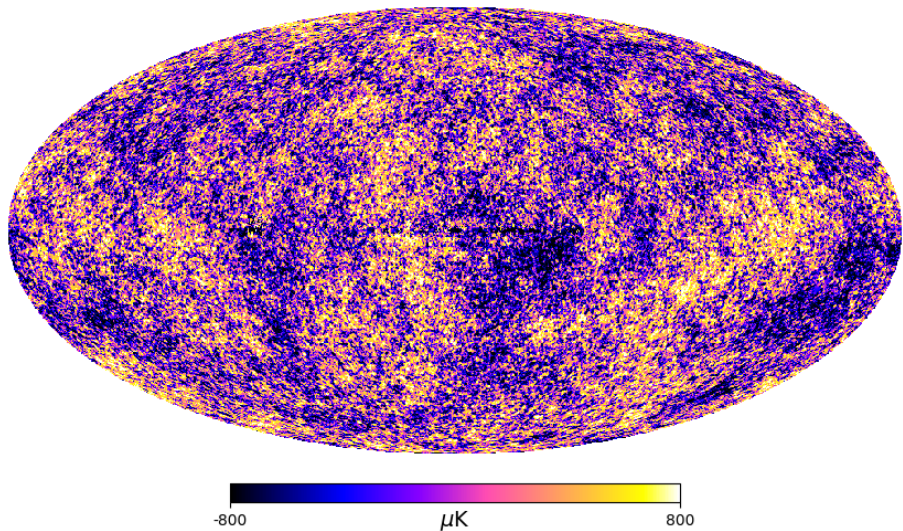


Figure 1: A flat, 2-D Mollweide projection of the Planck CMB temperature distribution around the sky. Note that the Mollweide projection is a projection of the 3-D sky onto flat space for ease of analysing whole sky maps.

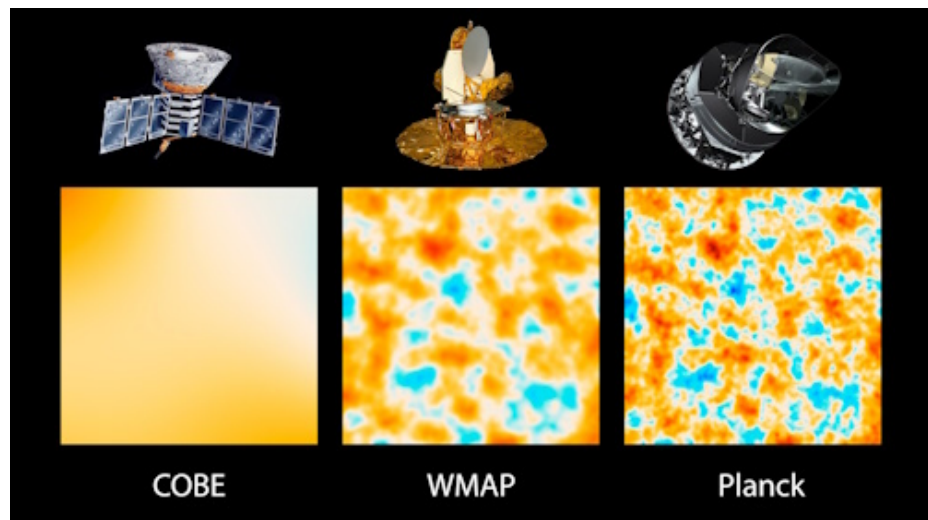


Figure 2: An image showing a portion of the CMB temperature sky map for the COBE (Cosmic Background Explorer), WMAP (Wilkinson Microwave Anisotropy Probe), and Planck satellites. COBE provided the first full sky measurement of anisotropy in the CMB, WMAP was launched in 2001 and increased these anisotropies for tighter constraints in parameter measurements which were constrained even more by the Planck satellite, launched in 2009. Highlighted specifically is the increase in resolution from each subsequent satellite, which shows the anisotropies in the temperature distribution. This increase was caused by greater sensitivity in the capabilities of these satellites. The scale of the anisotropies are on the order of -200 to $200\mu\text{K}$. *Image credit : LAMBDA – cosmicmicrowavebackground. https://lambda.gsfc.nasa.gov/education/graphic_history/microwaves.html*

Chapter 1

Inflation, Anisotropy, and the CMB Power Spectrum

The discovery of the CMB is an interesting story, an unexpected revelation that led to a large shift in the course of modern cosmology. The CMB was discovered in 1965 by physicists Arno Penzias and Robert Wilson using an antenna at Bell Labs, located in Holmdel, New Jersey. They used this antenna for sensitive microwave measurements of radio emissions from the Milky Way, and what resulted was a uniform excess temperature background of 2.726K.¹ They subsequently reduced all factors that could have contributed to this “noise” mechanically, and the background remained. At the same time, Princeton physicist Robert Dicke was working on an early iteration of the Big Bang theory based on the experimental results of Hubble that found the universe was expanding. These early theories predicted a cosmic microwave background. It was still under question whether or not this background would be isotropic.² Penzias and Wilson came in contact with Dicke, who characterized the source of this noise as evidence of the proposed cosmic microwave background.³ Nevertheless, given the limitations of the radio telescope measurements, their data suggested an isotropic CMB. It wasn’t until the first satellite measurements of CMB temperature maps were taken that the anisotropies were detected in 1989 by the COBE satellite, since the small variations in photon temperatures coming from the CMB are hard to distinguish, on the order of $\frac{\Delta T}{T} = 10^{-5}$.⁴ The highest resolution of these temperature maps come from the WMAP (launched in 2001) and Planck (launched in 2009) satellites.⁵ The detection of this anisotropy was highly important to the development of the field of cosmology, as it provided strong evidence for cosmic inflation, as well as allowed provided a way to estimate the cosmological parameters.⁶

In the Λ *CDM* model, our universe today consists of baryonic and dark matter, dark energy, and radiation, described by the dimensionless cosmological density

¹Penzias & Wilson (1965)

²Dicke, R. H., et al. (1965)

³Penzias & Wilson (1965)

⁴Penzias & Wilson (1965); Mather (1990)

⁵Mather (1990); Bennett, C. L., et al. (2013); Planck Collaboration, et al. (2020a)

⁶Schneider (2006)

parameters Ω_m , Ω_Λ , and Ω_r . Currently, we are in the Λ dominated epoch of the universe, as the expansion rate (a cosmological parameter called Hubble's constant) H_0 increases over time (the expansion accelerates). The current state of the universe is low density, allowing for life and even the writing of this thesis. If we reverse expansion to a state of high density, the universe would look very different, with a hot plasma of baryons and electrons, and light easily interacting with particles, unable to travel freely.⁷ If we look even further back to the very first minor fraction of a second of the universe's finite lifetime, it is predicted that the curvature of space in this period must be very nearly flat given that the current curvature of the universe is estimated to be close to flat, and any departure from flatness in the very early universe would greatly change the curvature we estimate today. This is called the "flatness" problem in cosmology. Nevertheless, this indicates a rapid inflation of space at this time to explain this "flattening".⁸ The near-isotropy of the CMB also indicates that the photons in the surface of last scattering must have been in some form of causal contact at a point in the early universe in order to be in thermal equilibrium. This "horizon problem" is further evidence the early universe must have undergone an exponential expansion prior to which the observable universe was extremely dense and smaller relative to its current size such that the edges of the surface of last scattering were in causal contact.⁹ The early exponential expansion of the universe indicated by the flatness and horizon problems is called the inflation theory of the universe, and is largely accepted today and a part of the Λ CDM model. Before inflation, when the observable universe was at a significantly smaller relative scaling, there were fluctuations of quantum fields of the universe to take into account. Inflation occurred very quickly given that the overall expansion of inflation is exponential in time, and during inflation the universe expanded by a factor of 10^{30} .¹⁰ After the universe inflated, the quantum fluctuations converted to matter and radiation density fluctuations.¹¹ Figure 1.1 displays a diagram of the history of the universe, highlighting the period of inflation, followed by slower expansion which leads to the cooling of matter to form atoms.

Inflation theory predicts that quantum fluctuations from the initial rapid inflation of the universe became matter density fluctuations when expanded to the large-scale. This created areas of slight over-densities and under-densities, which then give rise to a large portion of anisotropy within the CMB due to gravitational redshifting and a general thermal effect. Over-dense areas were hotter than under-dense areas, causing a higher relative photon temperature in overdense areas. However, photons from these overdense areas were subsequently gravitationally redshifted. Further, underdense areas were blueshifted.¹² This effect of gravitational redshifting, counteracted the general thermal temperature difference of overdensities and underdensities. A map

⁷Schneider (2006)

⁸Schneider (2006)

⁹Schneider (2006)

¹⁰Peebles (1993)

¹¹Schneider (2006)

¹²Peebles (1993)

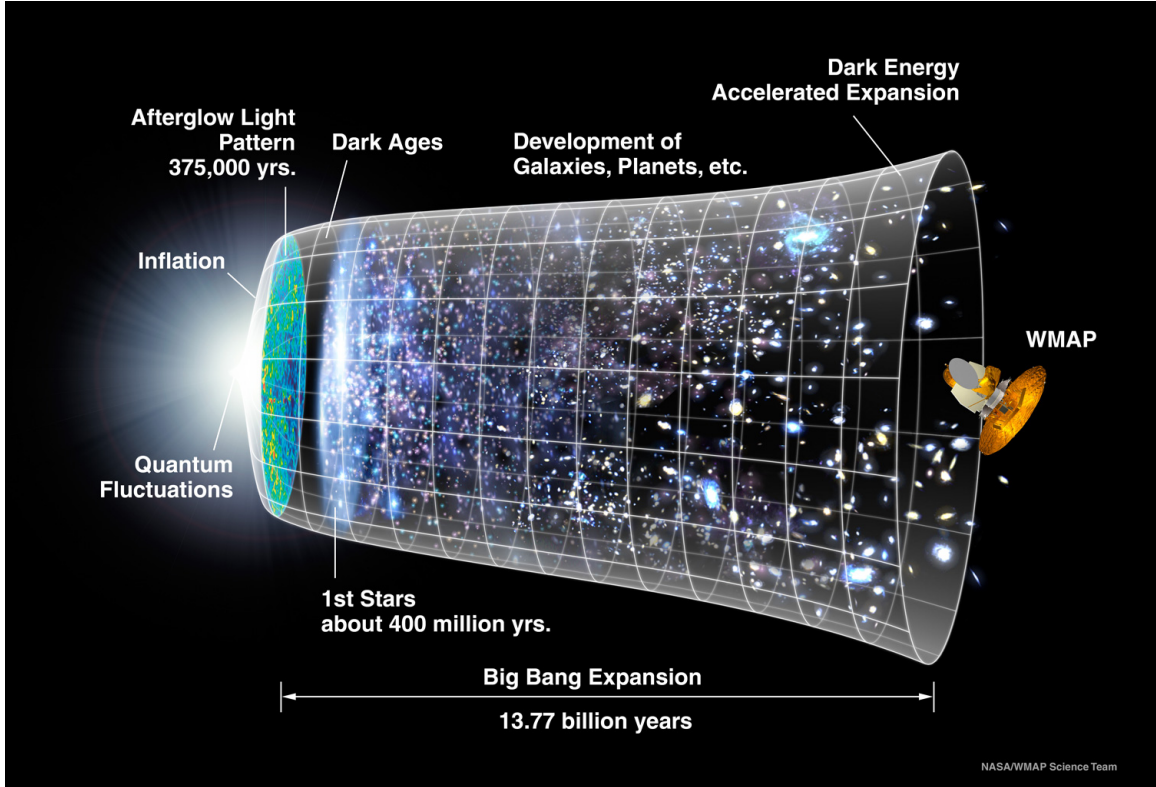


Figure 1.1: A diagram of the history of the universe in cosmological time, showcasing inflation, recombination, and the formation of the first large scale structures. The image begins at the instant of the Big Bang with quantum fluctuations and ends with the present day, where satellites such as WMAP measure the CMB. *Image credit: Timeline of the Universe Image, <https://wmap.gsfc.nasa.gov/media/060915/index.html>*

plotting the temperature differences of CMB photons is displayed in Figure 1.2.¹³ These temperature differences are usually plotted as $\frac{\Delta T}{T_{CMB}}$, where T_{CMB} is the average temperature of the CMB, 2.276K. Several other effects contribute to anisotropy, which will be discussed later.

Characterizing anisotropy in the CMB can be done in numerous ways, but the most prominent and useful for calculating cosmological parameters is with 2-point correlation functions and multipole expansions that characterize the intensity of anisotropy of the CMB on varying angular scales.¹⁴ This anisotropy intensity as a function of spatial wavelength of spherical harmonics (an increasing spatial wavelength corresponds to an increasing angular scale) is called the angular power spectrum of the CMB. The power spectrum can be thought of a plot of the intensity of anisotropies as a function of multipole moment, ℓ , which is inversely correlated to angular scale.¹⁵ The multipole moments correspond to an angular frequency at

¹³Peebles (1993)

¹⁴Jungman, G., et al. (1996)

¹⁵Callin (2006)

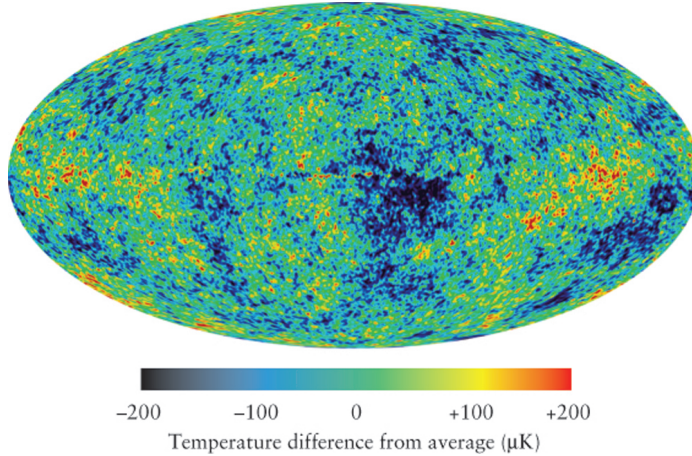


Figure 1.2: A Mollweide plot of CMB temperature differences (with no galactic foregrounds) from the average for data taken from the WMAP satellite. Note that fluctuations range on the scale of -200 to $200 \mu\text{K}$. *Image credit: The universes of max tegmark. (n.d.). <https://space.mit.edu/home/tegmark/wmap.html>*

which the fluctuations are averaged based on the spherical harmonics. Spherical harmonics are characterized by integer m and ℓ values, where m ranges from $-\ell$ to ℓ . The indices m and ℓ correspond to varying spherical harmonic functions based on angles θ and ϕ . Further, the spherical harmonic functions themselves make up an orthonormal basis for functions of θ and ϕ , which allows us to sum over their values in a multipole expansion. Figure 1.3 shows the spherical harmonic functions plotted for various combinations of ℓ and m values. One can see how increasing the multipole moment corresponds to a decreasing angular scale in the pattern of these harmonics.

The exact shape of the power spectrum is influenced by the various cosmological parameters: $\Omega_b, \Omega_c, m_\nu, H_0, \Omega_k$, and τ .¹⁶ These parameters and their dependencies will be further explored in Chapter 2. I will start by explaining the fundamental mathematical groundwork for this method of analysis, and then present calculations of the CMB power spectrum for the Planck 2018 satellite using my own code, comparing to other calculations of the power spectrum both by the Planck group and the healpy Python module. This method of power spectrum calculation will act as the basis for parameter extraction done in Chapter 2.

1.1 Determining the Power Spectrum

Any function defined on the surface of the sphere can be written in terms of spherical harmonics to a good approximation using a multipole expansion because they form an orthonormal basis in θ and ϕ .¹⁷ For our purposes, we can express $\frac{\Delta T}{T_{CMB}}$ for sky

¹⁶Jungman, G., et al. (1996)

¹⁷Callin (2006)

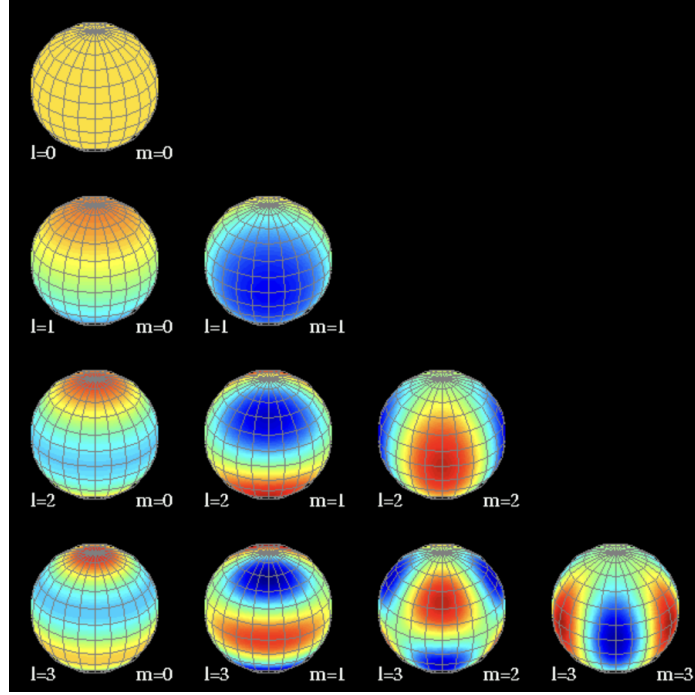


Figure 1.3: An image showing the spherical harmonics for various values of ℓ and m . One can see an oscillatory pattern on the sphere for increasing ℓ and m values. *Image credit: Harmonic multipoles and the CMB sky. (n.d.). <http://find.spa.umn.edu/pryke/logbook/20000922/>*

maps of the CMB in a multipole expansion as such:

$$\frac{\Delta T}{T_{\text{CMB}}}(\theta, \phi) = \sum_{\ell=0}^{\ell_{\text{max}}} \sum_{m=-\ell}^{+\ell} a_{\ell,m} Y_{\ell,m}.^{18} \quad (1.1)$$

In this equation, $Y_{\ell,m}$ represents spherical harmonics, and the $a_{\ell,m}$ are referred to as multipole coefficients. These multipole coefficients are analogous to Fourier coefficients in a Fourier expansion of a periodic signal in 1 dimension. Given pixelated data, they are estimated by the following relation:

$$a_{\ell m} = \frac{4\pi}{N_{\text{pix}}} \sum_{p=0}^{N_{\text{pix}}-1} Y_{\ell m}^*(p) \frac{\Delta T}{T_{\text{CMB}}}(p). \quad (1.2)$$

Here, p represents a generic point on the surface of the sphere with coordinates (θ, ϕ) .¹⁹ These coefficients are related to the CMB power spectrum by the following relation:

$$C_\ell = \langle |a_{\ell,m}|^2 \rangle \quad (1.3)$$

¹⁹Gorski, Krzysztof M., et al. (1999)

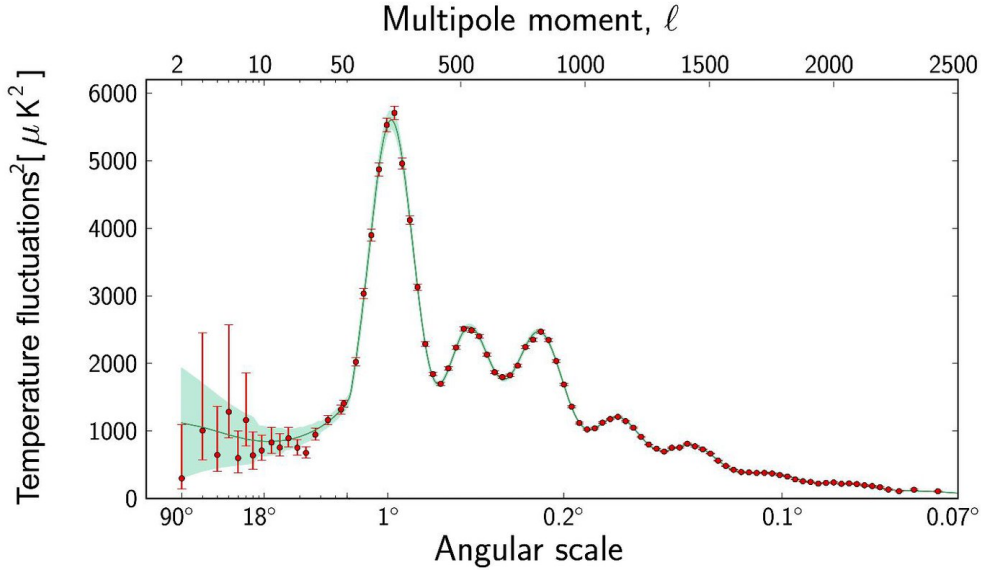


Figure 1.4: An image showing temperature fluctuations of the CMB plotted as a function of multipole moments and angular scale. These temperature fluctuations make up the “angular power spectrum” of the CMB. The solid line plot is the expected power spectrum curve. *Image credit: NASA. (n.d.-b). The Universe, summed up in a squiggly line. NASA. <https://www.jpl.nasa.gov/images/pia16879-the-universe-summed-up-in-a-squiggly-line>*

where the power spectrum is the ensemble average of the coefficients squared.²⁰ This “ensemble average” provides the expected value of the $a_{\ell,m}$ coefficients given a stochastic process of temperature variations around the sky. Under the assumption that we live in a universe where distinct portions of the sky are statistically independent at large distances, and where the temperature differences are stochastic, we can convert this result into an average over the coefficients squared over all values of m :

$$\hat{C}_\ell = \frac{1}{2\ell + 1} \sum_{m=-\ell}^{\ell} |a_{\ell m}|^2. \quad (1.4)$$

²⁰Mo, Houjun., et al. (2010)

Note that this is no longer a ensemble average. The factor of $\frac{1}{2\ell+1}$ comes from the fact that there are $2\ell + 1$ modes for each ℓ .²¹ The hat over the C_ℓ indicates the that we are averaging over all values of m and not all samples given that we only have one observable sample of a CMB, namely our universe's CMB. This is important for error analysis on the power spectrum and will be discussed more later in this chapter.

It should be noted that \hat{C}_ℓ is directly related to what is known in astrophysics as the 2 point correlation function.²² This 2 point correlation function measures the probability that two points share the same value and is a common measure of anisotropy. The power spectrum and the 2 point correlation function are related as follows:

$$C(\theta) = \sum_{\ell=2}^{\infty} \frac{2\ell+1}{4\pi} \hat{C}_\ell P_\ell(\cos(\theta)).^{23} \quad (1.5)$$

Here, the P_ℓ s represent the Legendre polynomials. The angular power spectrum and the 2-point correlation function contain essentially the same information, but for the purposes of determining the cosmological parameters, we will be using the angular power spectrum.²⁴ It should also be noted that a common convention is that the the power spectrum is plotted as the following:

$$\hat{D}_\ell = \frac{\ell(\ell+1)}{2\pi} \hat{C}_\ell.^{25} \quad (1.6)$$

This convention is done because it makes the features of the power spectrum graph and the anisotropy effects that contribute easier to see.²⁶ Notably, under this convention, the factor of $\ell(\ell+1)$ introduces a problematic point which occurs at $\ell = 0$, which will be apparent in my data later on.

1.2 Contributions to Anisotropy

The power spectrum of the CMB has a unique graphical structure shown in Figure 1.5. This graphical structure comes from multiple effects that contribute to the observable anisotropy that we see in the CMB temperature map. Largely, these effects can be labeled as primary, secondary, and tertiary anisotropy effects. Primary effects are ones that occur at recombination, when the CMB photons are released. Secondary effects occur from recombination up until the present, and tertiary effects are ones that occur in the present day like galactic foregrounds. The most notable primary effects are the Sachs-Wolfe effect relating to the redshifting of CMB photons from gravity as photon leave potential wells, which is impacted by matter over densities and under densities from baryonic acoustic oscillations, a general temperature shift

²¹Gorski, Krzysztof M., et al. (1999)

²²Peebles (1993)

²⁴Peebles (1993)

²⁵Mo, Houjun., et al. (2010)

²⁶Mo, Houjun., et al. (2010)

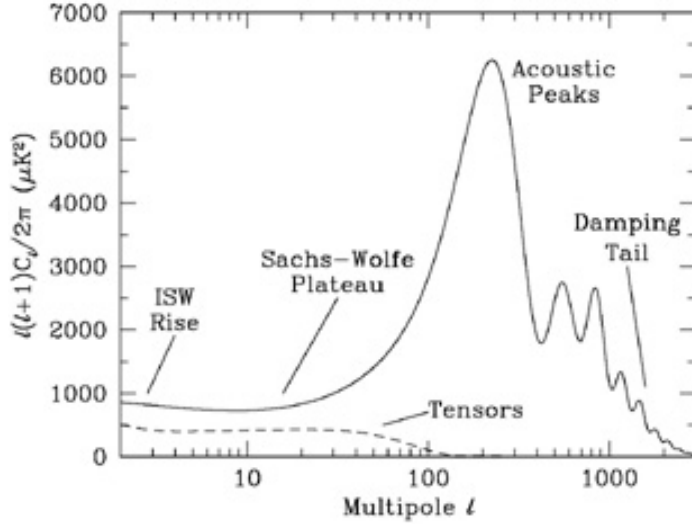


Figure 1.5: A plot of the CMB power spectrum with labels of each section. *Image credit: Scott, Douglas Smoot, George. (2004). Cosmic Background Radiation Mini-Review.*

in areas of over densities and underdensities, and Doppler shifting from the peculiar velocity of density fluctuations.²⁷ Notable secondary effects are the Sunyaev-Zel'dovic effect (resulting from Compton scattering by galaxy clusters and sources of plasma) and the integrated Sachs-Wolfe (ISW) effect both in the early and late stages.²⁸ Some of these can be seen in Figure 1.6 which shows exactly how various effects contribute to anisotropy in the CMB. I will not go over many tertiary effects, but the most important is the distortion of the CMB power spectrum by galactic foregrounds and other sources of radiation at microwave wavelengths.²⁹

Looking at the plot in Figure 1.5, there are several notable peaks that roughly decrease with increasing multipole. These are the acoustic peaks of the CMB power spectrum, and are caused by photons being released at extrema of baryonic acoustic oscillations. Baryonic acoustic oscillations are oscillating regions of overdensities and underdensities of baryons which fall in and out of dark matter potential wells. These oscillations function much like a sound wave from the time that the sound horizon overtakes the size of these overdensities, to the time of recombination.³⁰ The sound horizon is the comoving distance sound could travel from the Big Bang to a time before recombination.

Figure 1.7 shows a visual representation of a single one of these BAOs using the analogy of masses oscillating back and forth on springs and their subsequent temperature shift as a function of time. If photons exit at a maxima of these oscillations, they exit from an overdense region which subsequently redshifts the photons, decreasing their temperature. The opposite occurs for density minima which have a blueshifting

²⁷Tegmark (1995)

²⁸Tegmark (1995)

²⁹Tegmark (1995)

³⁰Hu

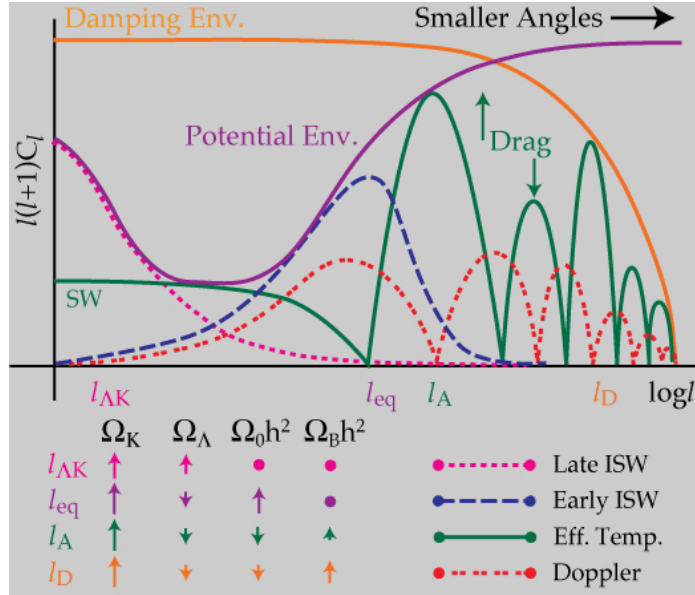


Figure 1.6: A plot showing anisotropy contributions to the CMB power spectrum with respect to the following effects: the early and late integrated Sachs-Wolfe effect, the baryonic acoustic oscillation effects, labeled as eff. temperature, and Doppler shifting from the baryonic acoustic oscillations. This plot also shows their dependencies on the cosmological parameters. *Image credit: W. Hu, N. Sugiyama, and J. Silk, The Physics of Microwave Background Anisotropies, Nature 386, 37 (1997).*

effect that increases the temperature contribution of the CMB photons relative to the redshifting effect.³¹ This gravitational redshifting is what is known as the ordinary Sachs-Wolfe effect, occurring at the time of recombination. There is also a general temperature shift that is caused by greater temperatures in areas of overdensities relative to areas of underdensities.³² This effect opposes the Sachs-Wolfe gravitational redshifting as areas of overdensities are blueshifted by this thermal effect and areas of underdensities are redshifted.

The impact of the Sachs-Wolfe effect and general temperature shift summed together on the power spectrum can be shown in Figure 1.6 in the line labeled effective temperature. Figure 1.6 shows the subsequent peaks and valleys given by the squared value of the temperature shifts, since either positive or negative ΔT give extra power at that angular scale. It should be noted that the temperature shifts shown in Figure 1.7 are a function of time whereas the temperature shifts in Figure 1.6 are plotted as a function of angular scale. Further, in Figure 1.7 these oscillations are plotted on the y-axis as $-\Delta T$, meaning the negative extrema represent compressions and the positive extreme represent rarefactions. The oscillations that occur in time are intimately related to the anisotropy that occurs as a function of angular scale. For a greater frequency of oscillation, the wavelength of the baryonic acoustic oscillations are reduced and vice versa for decreased frequency. Wavelength, along with the specific time of

³¹Hu

³²Tegmark (1995)

recombination set the angular scale at which these oscillations are imprinted.³³ The specific acoustic peaks of the power spectrum are essentially set by modes of compression or rarefaction of these oscillations. The first peak in particular occurs for the first compression mode of baryonic acoustic oscillations, which only has time to compress once before recombination, when photons are released in this compression mode (this compression mode is not even a full cycle of compression). Other modes are present and most are in the middle of oscillation when recombination occurs, but the extrema of the oscillations are imprinted in the peaks shown in Figure 1.6 as a function of angular scale, and stronger in anisotropy because of the combined thermal and gravitational effects at these points.³⁴ The reason why the peaks have different heights is because of damping and the fact that some modes are more present than others (namely the first compression mode is the strongest). Further, Figure 1.7 gets the idea that the baryons oscillate in time, but the amplitudes of these peaks as a function of time are not even as some compressions are stronger than others, and further a lot of the baryonic acoustic oscillation modes do not even go through a full cycle of oscillation before being released. Namely, the first peak does not go through this full oscillation.³⁵ So, while this figure is important for demonstrating the oscillating behavior of these baryons, it should be noted that this doesn't represent the full picture of how these oscillations in time and space are imprinted in the anisotropy of the CMB. Figure 1.6 captures the much more full picture of the contributions to anisotropy of the BAOs as a function of angular scale rather than an oscillation in time.

Figure 1.7 shows the temperature shift in time only from the general thermal

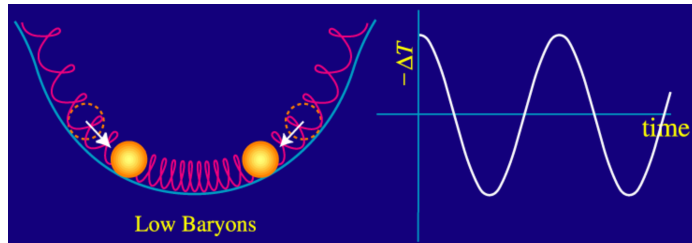


Figure 1.7: A diagram showing a visual analogy of baryonic acoustic oscillations, represented as masses on springs. The circles represent the baryons while the springs generally represent the force of gravity and opposing radiation pressure. These masses oscillate in a half pipe, moving in and out of a potential well just as baryonic acoustic oscillations. Also shown is the subsequent temperature shift as a function of time for a low baryon density model. *Image credit: W. Hu, Wayne Hu's Tutorials, <http://background.uchicago.edu/>*

effect of BAOs with low baryon content for a single wavelength mode. When baryon content is included in the model, it produces an temperature shift curve similar to Figure 1.8, again only for a single wavelength mode. As a reminder, both Figures

³³Hu

³⁴Hu

³⁵Hu

1.8 and 1.7 are plotted as $-\Delta T$ on the y axis, meaning compression maxima are in the negative y regime and rarefaction maxima are in the positive y regime. The extrema that represent compression are raised in absolute value over the extrema that represent rarefactions. This raising of compression extrema occurs because increased baryon density corresponds to a greater effect of gravity resisting the motion of the baryon-photon fluid as it oscillates in and out of the dark matter potential wells, compressing the fluid more as it falls into areas of greater potential energy, in an effect called baryon drag.³⁶ Baryon drag subsequently reduces the level of rarefaction in the opposite extrema as well. As a result, when the wavelength modes are combined and translated to anisotropy as a function of angular scale, we see a lowered height of even peaks and raised height of odd peaks of the power spectrum, given that even peaks represent rarefaction modes and odd peaks represent compression modes.³⁷ Figure 1.6 shows this effect represented by the arrows labeled “Drag”. The overall effect of lowering even peaks and raising odd peaks is called baryon loading.³⁸ Baryon loading creates a large dependence of the acoustic peak heights on the baryon density parameter, Ω_b , which will be discussed further in Chapter 2.³⁹

There is also an effect of Doppler shifting on CMB anisotropies at the time of recombination. For each particular wavelength, the velocity of the baryonic acoustic oscillations were out of phase by a 1/4 period of oscillation with the temperature shifts caused by mass overdensities and underdensities.⁴⁰ This phase shift occurs because the turning points of the baryonic acoustic oscillations occur at the extrema of the baryon-photon fluid oscillations, where the subsequent temperature shift is greatest. Meanwhile, maximal velocity shift of the photon-baryon fluid occurs in between these extrema since the turning points are where the velocity is minimal.⁴¹ When photons were released at recombination, this movement caused a subsequent Doppler shift and hence temperature shift depending on the movement of the baryon-photon fluid towards or away from our point of observation.⁴² Photons released from fluid moving away are redshifted, while photons moving towards us are blueshifted corresponding to a respective decrease and increase in temperature. The pattern this effect has on the angular power spectrum can be seen in Figure 1.6 by the red dotted line labeled as “Doppler”.⁴³

As can be seen from Figure 1.6, the CMB power spectrum’s peaks generally decrease in height as the angular scale decreases and multipole moments correspondingly increase. The baryon-photon fluid is imperfect such that at smaller scales, photons Compton-scatter and randomly “walk” through the fluctuations. These photons have a mean free path, and as this mean free path becomes comparable to the size of the

³⁶Hu³⁷Hu³⁸Hu³⁹Hu⁴⁰Hu⁴¹Hu⁴²Tegmark (1995)⁴³Hu

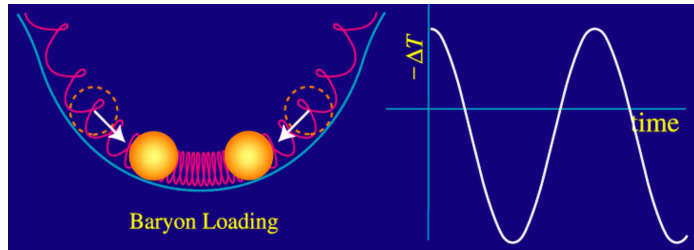


Figure 1.8: A plot of the temperature anisotropy curves from the baryonic acoustic oscillations, where baryon content is included and creates an overall effect of baryon loading. *Image credit: W. Hu, Wayne Hu's Tutorials, <http://background.uchicago.edu/>*

wavelength of BAOs, the anisotropies dampen out given the random movement of photons and loss of the fluid-like behavior at smaller angular scales.⁴⁴ What results is a near exponential decrease in anisotropy contributions of BAOs as angular scale decreases, and creates what is called the famous “Silk damping tail” of the CMB power spectrum, as shown by the yellow damping tail in Figure 1.6.⁴⁵

To discuss some secondary effects, the integrated Sachs-Wolfe effect is split up into late and early stages.⁴⁶ The early ISW effect is caused by gravitational redshift just after recombination as photons exited the surface of last scattering and up until matter completely dominated the universe.⁴⁷ This effect primarily arises due to the universe not being fully matter dominated at recombination. If the universe is completely matter dominated, potential wells do not change significantly, contributing to anisotropy of CMB photons.⁴⁸ Because this was not fully the case and the fact that the universe expands adiabatically, radiation pressure decays gravitational potentials due to the counteracting force of the radiation and the gravitational force of matter. This effect makes the potential fluctuation from BAOs decay at particular wavelengths as the sound horizon expands past the wavelength, contributing to anisotropy in the CMB.⁴⁹ The early ISW effect impacts the smaller multipoles and larger angular scales because the sound horizon of the surface of last scattering is much larger now than it was at recombination. The early ISW effect is shown in Figures 1.5 and 1.6. Further, it creates a bump in the low multipoles of the power spectrum.

The late ISW effect occurred when accelerated expansion of the universe began (as dark energy dominated the universe).⁵⁰ In the matter dominated epoch, gravitational potentials did not decay significantly as the universe expanded. This stagnant evolution of potentials is not the case for an accelerated expansion, as spacetime stretches,

⁴⁴Hu

⁴⁵Hu

⁴⁶Wright

⁴⁷Hu

⁴⁸Hu

⁴⁹Hu

⁵⁰Cabass, Giovanni, et al. (2015)

changing potential wells by smoothing them out.⁵¹ If there was a change in a potential as a photon crossed a well, there would be a residual temperature shift because the effects of blue-shifting as the photon enters the well, and red-shifting as it leaves do not cancel out.⁵² The smoothing of the potential wells effectively blue-shifts the light as spacetime contracts. The late ISW effect mostly impacts multipoles less than $\ell = 100$ (corresponding to the largest angular scales) for reasons similar to the early ISW effect, because the sound horizon size was significantly larger when dark energy first dominated the universe than at recombination.⁵³ The late ISW effect creates a sloped increase in anisotropy towards the zeroth multipole. This can be seen in Figures 1.5 and 1.6. The late ISW effect acts as evidence for the presence of dark energy, and is sensitive to the curvature parameter.⁵⁴

The next effect we will address is the Sunyaev-Zel'dovic effect. The Sunyaev-Zel'dovic effect occurs because of bound electrons interacting with CMB photons (i.e. Compton scattering) after the CMB was released.⁵⁵ When CMB photons interact with plasma, depending on the relative peculiar velocity (meaning the velocity relative to the Hubble flow) of the material, energy is injected into them. This injection of energy due to the peculiar velocity of plasma is the kinematic Sunyaev-Zel'dovic effect.⁵⁶ Further, electrons can inject energy into CMB photons because of their relative temperature, causing the thermal Sunyaev-Zel'dovic effect.⁵⁷ Non-thermal electrons can also scatter CMB photons in sufficiently close to relativistic electron gases, creating the non-thermal Sunyaev-Zel'dovic effect.⁵⁸ As a result of these effects, the CMB is brighter in areas where there has been a lot of scattering and interactions. This can largely indicate the presence of galactic bodies and other reservoirs of hot plasma.⁵⁹ Roughly speaking, the Sunyaev-Zel'dovic effect stretches and compresses the power spectrum towards higher multipoles ($\ell > 300$). Higher multipoles are impacted more because of the fact that galaxy clusters are more localized and aren't usually much greater than 10 Mpc across. This corresponds to the effect contributing to smaller angular scales, and higher multipoles. The Sunyaev-Zel'dovic effect can be used to identify galactic clusters, but also acts as a probe of Hubble's constant because it can tell us how far away these galactic clusters are.⁶⁰

There is also an effect of CMB photons Thomson scattering from the period of the universe where it was first reionized after recombination and until now. Photons subsequently deflect due to these ions which reduces anisotropies of the power spectrum. This will be discussed further in Chapter 2, as we define the reionization optical depth τ . Essentially this effect reduces the heights of all the peaks of the power spectrum, which will also be shown in Chapter 2 once I characterize τ .

⁵¹Cabass, Giovanni, et al. (2015)

⁵²Wright

⁵³Hu

⁵⁴Hu

⁵⁵Peebles (1993)

⁵⁶Birkinshaw

⁵⁷Birkinshaw

⁵⁸Birkinshaw

⁵⁹Peebles (1993)

⁶⁰Peebles (1993)

Tertiary effects can be described as contributions to anisotropy from galactic foregrounds and other sources of microwave radiation at microwave wavelengths.⁶¹ This requires “masking” CMB temperature maps. Masking is done by subtracting pixels that contain overwhelming contributions to anisotropy caused by sources other than the CMB. These contributions contaminate CMB maps by dimming the relevant primary and secondary contributions, which makes calculations less accurate.⁶² Producing a mask is done by taking Planck satellite data of galactic dust around the sky at different frequency bands, and matching it with CMB anisotropies to see where the contamination is occurring.⁶³

Before determining the CMB power spectrum, I had to load CMB data from the Planck 2018 release. These data came with a slight contamination in that there were residual temperature shifts from galactic foregrounds. In order to properly determine the power spectrum, this galactic contamination had to be masked. Luckily, the Planck Commander release has a mask available for download that takes care of this.⁶⁴ Nevertheless, there are still some leftover anisotropy contributions due to galactic foregrounds that are unavoidable due to the fact that the masks are imperfect and do not cover all galactic dust. Ultimately, the map that I determined the power spectrum for is shown in Figure 1.10 with the mask applied. This mask was applied using `healpy`, a python module that allows for easy loading and manipulation of CMB maps in the HEALPix format (more below).

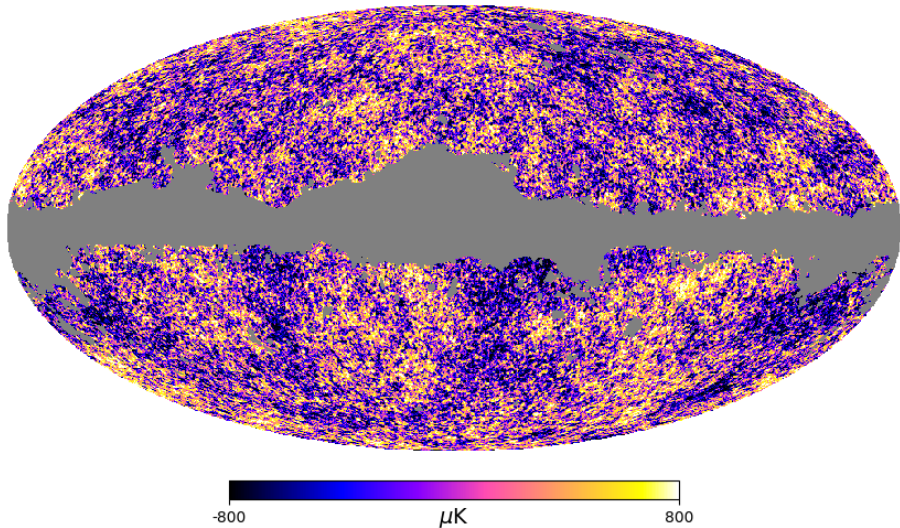


Figure 1.9: A Mollweide projection of CMB temperature anisotropies (in units of μK from $-800\mu K$ to $800\mu K$) with the galactic foreground masked. This mask was taken from the Planck 2018 data release.

⁶¹Tegmark (1995)

⁶²Planck Collaboration, et al. (2020a)

⁶³Planck Collaboration, et al. (2020a)

⁶⁴Planck Collaboration, et al. (2020a)

1.3 Methods of Calculation

CMB maps are typically released in the HEALPix format, which sections off equal area portions of the sphere using isolatitude rings for each spherical harmonic. This allows for easy and fast generation of the spherical harmonic functions and manipulation of functions with a spherical topology.⁶⁵ Given that the summation in Equation 1.2 runs over all the pixels of the input CMB temperature map, it naturally takes a really long time to produce the results of the power spectrum. This is eased by the HEALPix formatting, letting one sum over each sectioned off area of the sphere for the coefficients. Essentially, this reduces the number of sums to be performed based on an input resolution that pixelizes the spherical map. In order to produce the power spectrum of the CMB, I wrote python code using Equation 1.2 to first determine the multipole coefficients $a_{\ell,m}$. I then used Equation 1.4 to turn these coefficients into power spectrum values, C_ℓ for each multipole, ℓ . Despite using the HEALPix format, this still took a very long time to generate, resulting in several optimizations required to output the spectrum. To make calculations faster, I used a matrix definition of the spherical harmonics generated by the healpy library to do all of the summations over each pixel in matrix form to calculate the multipole coefficients. This matrix version of the spherical harmonics are pre-calculated spherical harmonic functions put onto HEALPix pixels by healpy. The healpy library allows for fast calculations of the power spectrum. However, for the purpose of my research, I only used the spherical harmonic functions that the package adds, and developed the rest of my code separately using Equations 1.2 and 1.4. I used the healpy-calculated power spectrum plot to compare to my own, and the two are in astounding agreement. I also plotted the power spectrum produced by the Planck 2018 collaboration, and produced in their data release. Both plots are shown in Figures 1.11 and 1.12. The code runs much faster than it did initially, but still takes a significant amount of time to produce the power spectrum from the Planck 2018 CMB data, despite my optimizations. Initially it took days to produce just the first 100 multipoles, but now it takes roughly 17 hours to 1 day to generate 1000 multipoles on an ASUS Windows laptop. As a result, I only plotted the first 1000 multipoles, which provides the first three acoustic peaks, which are the most important for determining cosmological parameters (discussed more in chapter 2). Further, this spectrum is plotted for every 5 values of ℓ , whereas the healpy plot is plotted for every ℓ .

The power spectrum determined by the Planck group and the ESA is included with the data from the Planck Satellite. This Planck power spectrum provides a good check of the accuracy of both the healpy module and my own code. Plotted against my power spectrum determination is the power spectrum determined by the Planck group in Figure 1.12. This shows that for higher multipoles, my plot deviates from true curve. This is because I had to correct for the “beam width”.⁶⁶ The beam width is an angular scale that describes the angular resolution of the Planck satellite. On smaller scales, blurring of sources begins to occur. This beam can be approximated

⁶⁵Gorski, Krzysztof M., et al. (1999)

⁶⁶Zonca (2020)

in several ways, but for the purposes of this paper, we can approximate the beam as a 2D Gaussian. Luckily, there is an easy way to utilize the `healpy` package to make this correction using the `healpy Gauss` beam function.⁶⁷ For the purposes of this paper, I used the `healpy` package for beam correction, since I am more concerned with estimating the cosmological parameters than with approximating the beam. Figure 1.13 shows the plot of my calculations of the power spectrum, the `healpy` calculated spectrum, and the correct spectrum given by the Planck 2018. One can see that anisotropies increase greatly at lower and lower angular scales due to the limits of the beam resolution. This beam correction slightly alters the heights of the peaks but is fixed with the Gaussian approximation. The first 3 peaks of the plot I produced now match precisely with the Planck group's calculations.

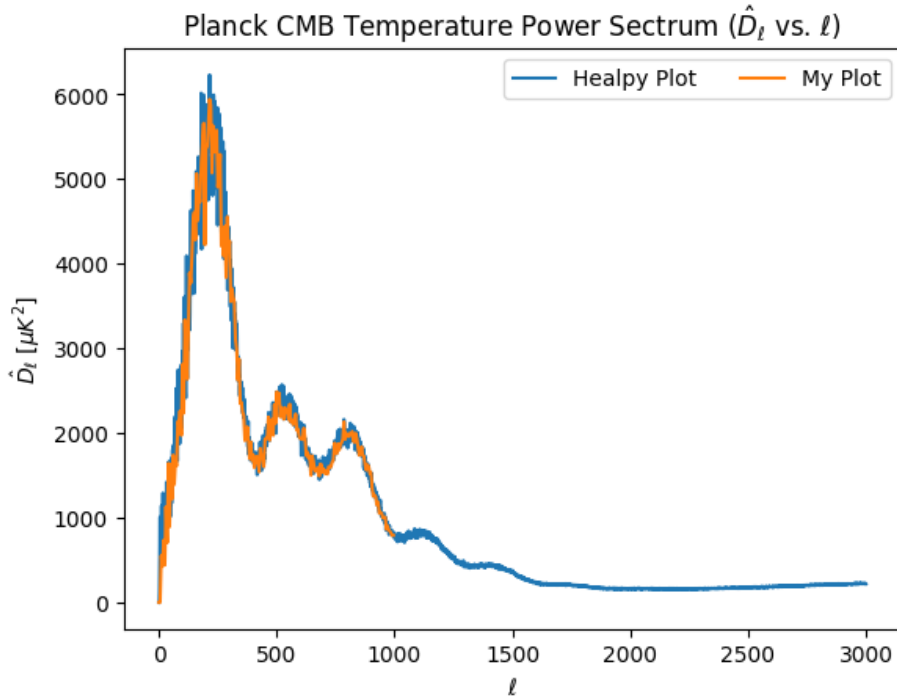


Figure 1.10: A figure showing the temperature power spectrum of the CMB plotted with the methods used in this paper and the `healpy` package. It is plotted as D_ℓ vs. multipole moment ℓ . Note that my code is plotted for every 5 multipoles whereas the `healpy` code is plotted for every multipole and that this is a line plot.

1.4 Error Estimation

Error estimation on the CMB power spectrum can be done in a number of ways, incorporating various contributions to uncertainty. The most notable source of uncertainty in the power spectrum arises due to cosmic variance.⁶⁸ Cosmic variance is an inherent

⁶⁷Zonca (2020)

⁶⁸Gerbino, Martina, et al. (2020)

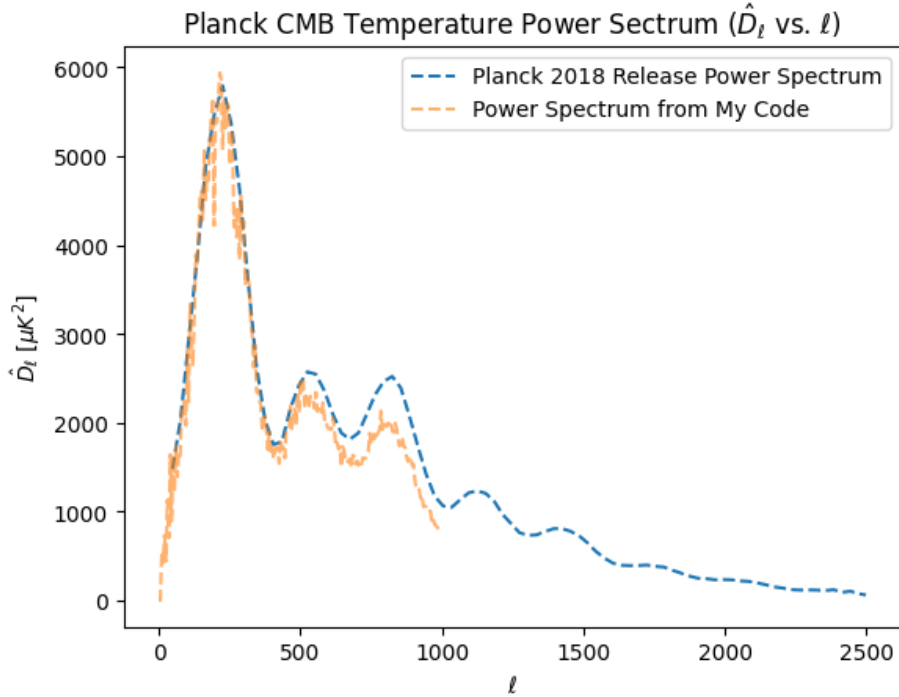


Figure 1.11: A figure showing the temperature power spectrum of the CMB plotted with the methods used in this thesis and the power spectrum from the Planck 2018 data release.

uncertainty in our measurements of the universe, produced by the fact that we only have the ability to measure the CMB from one location in the universe. This limits the statistical variety of our sampling and thus introduces an inherent error.⁶⁹ The ergodic hypothesis states that different regions of the sky separated at large distances are statistically independent.⁷⁰ If we are to assume the ergodic hypothesis to be true, as we sum over varying angular resolutions that correspond to spherical harmonics with indices/multipole moments ℓ and m as done in Equation 1.2, error should relatively decrease with increasing multipoles, by a factor of $\sqrt{\frac{2}{2\ell+1}}$.⁷¹ Given that there are $2\ell+1$ coefficients at any ℓ , this error becomes a factor in our expression for \hat{C}_ℓ , and will appear in the final expression for the cosmic variance. It should be noted that the error in switching from the theoretical true power spectrum C_ℓ , to the power spectrum we are familiar with, \hat{C}_ℓ , is the error associated with cosmic variance, and is given by the following expression from Gerbino, Martina, et al. (2020):

$$\langle (\frac{\hat{C}_\ell - C_\ell}{C_\ell})^2 \rangle = -1 + \frac{1}{(2\ell+1)^2 C_\ell^2} \sum_{mm'} \langle a_{\ell m} a_{\ell m}^* a_{\ell m'} a_{\ell m'}^* \rangle. \quad (1.7)$$

⁶⁹Gerbino, Martina, et al. (2020)

⁷⁰Gerbino, Martina, et al. (2020)

⁷¹Gerbino, Martina, et al. (2020)

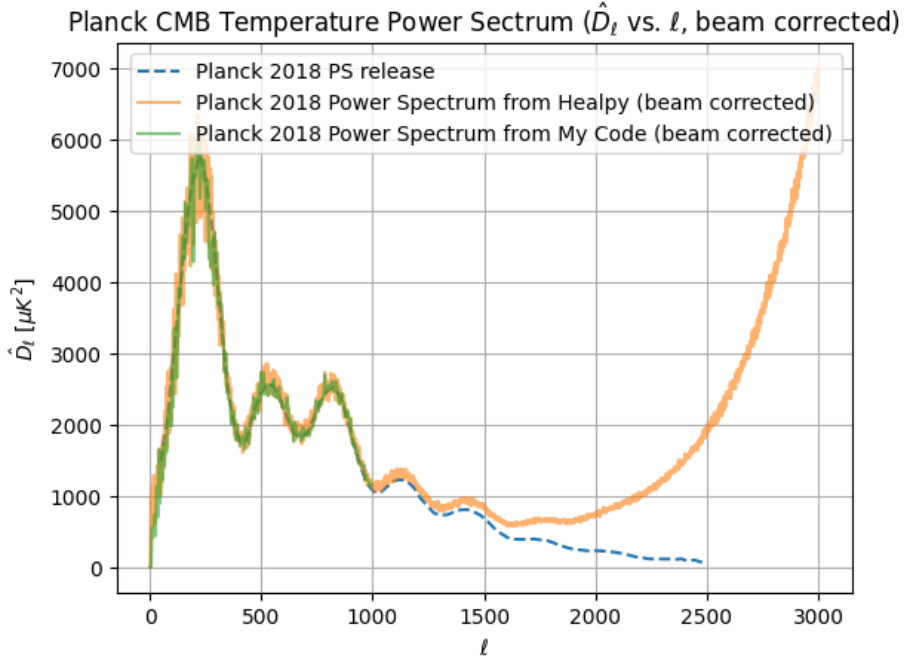


Figure 1.12: The temperature power spectrum of the CMB plotted with the methods used in this thesis, the power spectrum calculated with healpy, and the power spectrum from the Planck 2018 data release. The plot corresponding to my code and the healpy calculated spectrum are corrected for the beam using a 2D Gaussian approximation.

As a reminder, note that \hat{C}_ℓ is the observed power spectrum and C_ℓ is the “true” power spectrum. The reason why we see two sets of multipole coefficients multiplied together is because of the combination of \hat{C}_ℓ and C_ℓ . A full derivation of the final expression for cosmic variance is given by Gerbino, Martina, et al. (2020), but ultimately, using Wick’s theorem to expand the above summation of multipole coefficients, we end up with the following expression:

$$\langle \hat{C}_\ell - C_\ell \rangle = \sqrt{\frac{2}{2\ell+1}} \langle C_\ell \rangle = \sqrt{\frac{2}{2\ell+1}} \hat{C}_\ell. \quad (1.8)$$

Assuming the ergodic hypothesis, we can replace the ensemble average of the true power spectrum, $\langle C_\ell \rangle$, with the observed power spectrum, \hat{C}_ℓ .⁷² Here we see another factor of $2\ell+1$, representing the number of multipole coefficients. If we define: $D_\ell = \frac{\ell(\ell+1)}{2\pi} C_\ell$ and $\hat{D}_\ell = \frac{\ell(\ell+1)}{2\pi} \hat{C}_\ell$, we can substitute for C_ℓ and \hat{C}_ℓ to get the same expression for \hat{D}_ℓ . This is done in order to get the exact errors in the power spectrum plots I have produced thus far. Making this substitution we have the following relation:

$$\langle \hat{D}_\ell - D_\ell \rangle = \sqrt{\frac{2}{2\ell+1}} \hat{D}_\ell. \quad (1.9)$$

⁷²Gerbino, Martina, et al. (2020)

This expression defines the error due to cosmic variance for my plots of the power spectrum in terms of D_ℓ vs. ℓ rather than C_ℓ . However, because I used a galactic mask to delete a portion of temperature data, in reality the data I used covered only approximately 77.9% of the sky. This means we have to adjust the final expression shown in Equation 1.9 to account for limited sky coverage. To a good enough approximation, we can adjust the equation above by a factor of $1/f_{\text{sky}}$ where f_{sky} is the fraction of the sky that my data covered ($f_{\text{sky}} = 0.779$).⁷³ Ultimately, the final expression that I used for the error due to cosmic variance comes out to be:

$$\langle \hat{D}_\ell - D_\ell \rangle = \sqrt{\frac{2}{2\ell + 1}} \frac{1}{f_{\text{sky}}} \hat{D}_\ell. \quad (1.10)$$

What results are the error bars shown in Figure 1.14, which are relatively larger for the lower multipoles as expected. When plotting the Planck-calculated errors including measurement errors and the error from cosmic variance against my calculations, the result is in Figure 1.15. The Planck errors are smaller which makes sense because they are averaged over several multipoles for each point which reduces the uncertainty from cosmic variance for their plot points. My plot in Figure 1.15 shows the error bars for each multipole, however, with no averaging occurring.

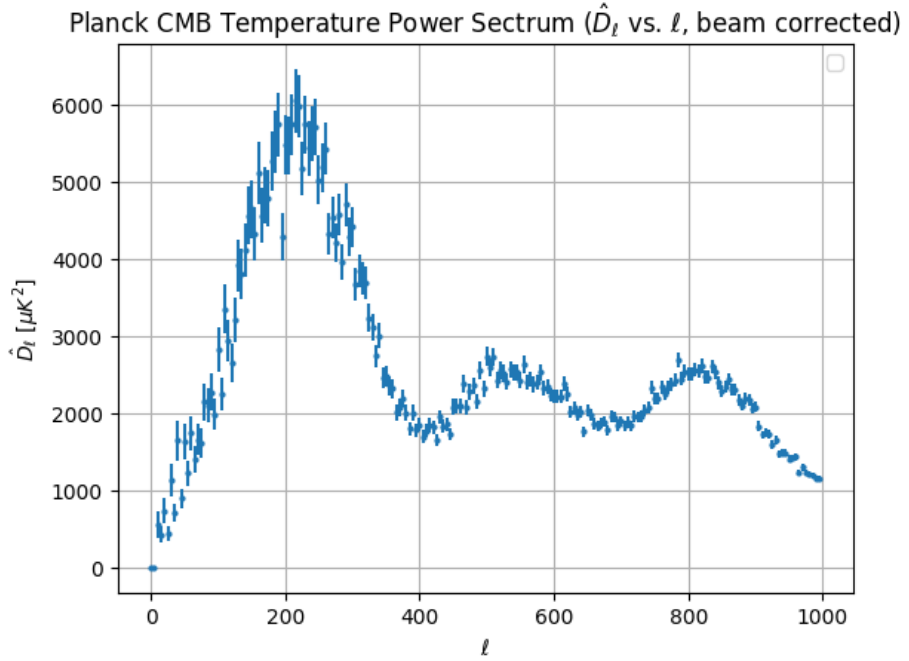


Figure 1.13: The temperature power spectrum of the CMB plotted with the methods used in this paper both beam corrected and with error bars that show the magnitude of error estimated from cosmic variance.

⁷³Gerbino, Martina, et al. (2020)

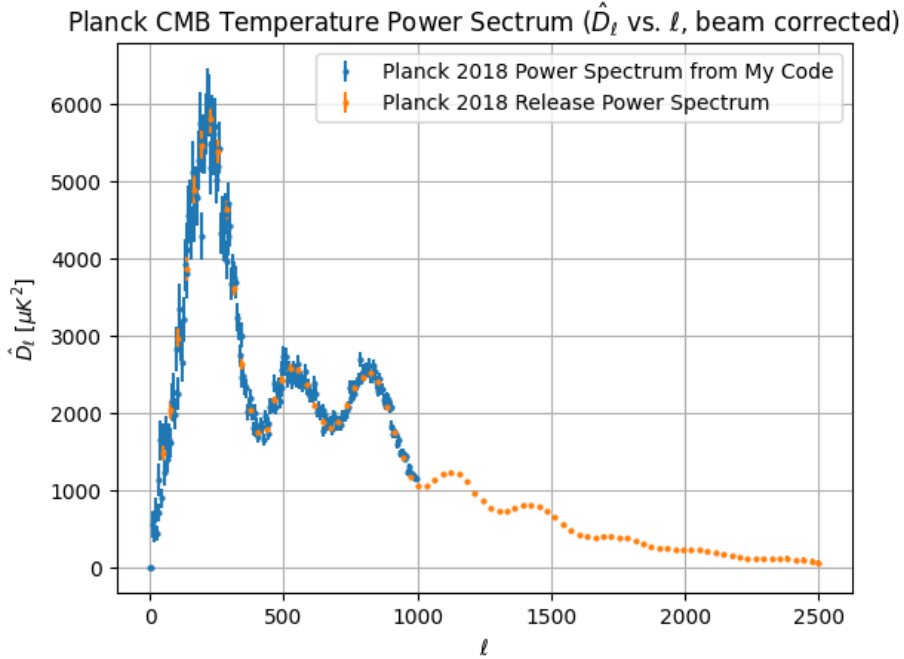


Figure 1.14: The temperature power spectrum of the CMB plotted with the methods used in this paper both beam corrected and with error bars that show the magnitude of error estimated from cosmic variance, as well as the Planck 2018 release power spectrum with errors accounting for measurement noise and cosmic variance.

Cosmic variance is the main source of error I will be considering in this thesis. The other main source of error to consider is the measurement errors of the Planck satellite. This error is negligible (below 1%) compared to that of cosmic variance, and thus won't be considered in this thesis.⁷⁴ The Planck collaboration has spent a lot of time correcting for noise errors in their satellite and have thus reduced them significantly such that they don't impact parameter estimates noticeably.⁷⁵ Other contributions to error come largely from galactic foregrounds adding noise to the CMB map. Though a lot of this was subtracted in the process of masking the CMB map, the provided Planck maps are not perfect and there likely still remains some contributions to anisotropy from galactic foregrounds. There is not a straightforward way to estimate this error, so this uncertainty is not included for the purpose of this thesis.

⁷⁴Ade, P. a. R., et al. (2014)

⁷⁵Ade, P. a. R., et al. (2014)

Chapter 2

Parameter Determination

To generate an analytical form of the power spectrum with a dependence on the cosmological parameters, equations describing the evolution of densities from contributions of dark energy, neutrinos, baryons, cold dark matter, and radiation must be simultaneously solved.¹ These equations are usually called “Boltzmann transfer equations” because they describe a change over time of some quantity in a thermodynamic system. Performing these calculations is not easily done in the span of time writing this thesis, but luckily there is a package for Python that solves these Boltzmann transfer equations and generates an analytical form of the power spectrum by pre-selecting cosmological parameters. A package that does this is called CAMB, which stands for “Code for Anisotropies of the Microwave Background”.² The analytical form that is produced can be matched with the observational data to estimate the cosmological parameters. In order to fully determine the cosmological parameters with proper errors, a package called CosmoMC is often used. This package runs a Monte-Carlo Markov Chain process on 6 selected cosmological parameters, randomizing them and seeing which fit the input data the best.³ Effectively, CosmoMC produces Markov chains for varying 6 parameters, which can then be analysed by an associated package called getdist.⁴ Then estimates of the parameters themselves can be obtained along with errors associated in the fitting process. This process is the basic method of how most cosmological parameter measurements from CMB data have been done, including by the Planck group in their 2013, 2015 and 2018 papers.⁵ CosmoMC will be discussed further in Chapter 3.

In the Λ CDM model there are 6 independent parameters from which the model is defined. The choice of these parameters is somewhat arbitrary since the full list of parameters from which they may be chosen are largely dependent on each other.⁶ For the purpose of this paper, the six dependent parameters I will be choosing are the preset dependent parameters in the CAMB code, which are very important in

¹Planck Collaboration, et al. (2014)

²Planck Collaboration, et al. (2014)

³Planck Collaboration, et al. (2020b)

⁴Planck Collaboration, et al. (2014)

⁵Planck Collaboration, et al. (2020b)

⁶Planck Collaboration, et al. (2020b)

the ΛCDM model. Note that all of these parameters are defined at the present day. These 6 base parameters are listed in Table 2.1.

I will begin by delving into the meaning and significance of each of the six cho-

Table 2.1: Planck 2018 Parameters⁷

Parameter Symbol	Parameter Name
H_0	Hubble's Constant (Current expansion rate)
Ω_b	Baryon Density Parameter
Ω_c	Dark Matter Density Parameter
m_ν	Summed Neutrino Mass
Ω_k	Curvature Parameter
τ	Reionization Optical Depth

sen parameters, and qualitatively show what increasing or decreasing each parameter does to the power spectrum using the CAMB code. For each of these experiments, one parameter is shifted at a time, while the other five are kept constant. Also listed will be some “dependent” parameter values (not within the six I have chosen as the independent parameters), and how they change with regards to the base parameters. These parameters include the vacuum energy density/dark energy density, Ω_Λ , the radiation density, Ω_r (including contributions from photons and neutrinos), the matter density, Ω_m , and the age of the universe, t_0 , and are listed in Table 2.2. Ω_Λ , Ω_r , and Ω_m give a better idea of the total contents of the universe according to the ΛCDM model. It is important to note that Ω_m includes both baryonic and dark matter, while Ω_r includes neutrinos and photons. The age of the universe is important because it is an easy parameter to match with observations. For instance, if we observe stars that are older than the age of the universe, clearly something is inconsistent with the model we are working with.

Following these experiments, I will then show the consistency of the power spectrum I generated in Chapter 1 with the power spectrum generated by CAMB using Planck 2018 parameters, showing how well my determination of the power spectrum is correspondent to these parameter values. This process will be the primary method of parameter extraction for this thesis. These methods of parameter extraction can be extended by the use of CosmoMC to get more accurate parameters with errors, which will be discussed further in Chapter 3.

2.1 Density Parameters

In order to define what these parameters represent, it is important to revisit some basic cosmological principles. The Friedmann expansion equations describe the large-scale evolution of the universe over time in its expansion and physical contents based on Einstein's cosmological principle and the Einstein equation of gravity which is the

Table 2.2: Dependent parameters discussed in this thesis.

Parameter Symbol	Parameter Name
Ω_Λ	Dark Energy Density Parameter
Ω_r	Radiation Density Parameter
Ω_m	Matter Density Parameter
t_0	Age of the Universe

basis of Einstein's general relativity. These equations are as follows:

$$\left(\frac{\dot{a}}{a}\right)^2 = \frac{8\pi G}{3}\rho - \frac{kc^2}{a^2} + \frac{\Lambda}{3}, \quad (2.1)$$

$$\left(\frac{\ddot{a}}{a}\right) = -\frac{4\pi G}{3}\left(\rho + \frac{3P}{c^2}\right) + \frac{\Lambda}{3}.^8 \quad (2.2)$$

These are effectively the equations of motion of the universe. The variable a represents the “scale factor” of the universe, which is intimately related to the expansion rate $H(t) = \frac{\dot{a}}{a}$ noting that a is dimensionless.⁹ For a better idea of what this scale factor represents, the distance between otherwise non-moving points in the universe scales by a as the universe expands, characterizing the overall expansion of the universe at a given time. The scale factor is defined such that $a(t_0) = 1$, where the value of the expansion rate today is precisely the Hubble constant. Further, ρ is the density of radiation, baryonic matter, and dark matter, which implies $\rho = \rho_r + \rho_m + \rho_c$.¹⁰ The variable k represents the spatial curvature of the universe, and is intimately related to the dimensionless curvature parameter. The constant Λ is the famous cosmological constant which is a constant of integration corresponding to the influence of dark energy on expansion.¹¹ Interestingly, Einstein disregarded this constant at first, and only recently was it discovered that this constant must be nonzero (the CMB power spectrum acts as evidence for this, although it was discovered that the constant is nonzero by observations of type 1a supernovae). We can also define a density due to dark energy, which is given by the following formula:

$$\rho_\Lambda = \frac{\Lambda}{8\pi G}.^{12} \quad (2.3)$$

From Equation 2.1, the density at which $k = 0$ can be calculated. This corresponds to a completely flat universe, and provides a characteristic density of the universe, $\rho_{cr,0}$, defined at the present day, using our construction of ρ_Λ . This “critical density”

⁸Schneider (2006)

⁹Schneider (2006)

¹⁰Schneider (2006)

¹¹Schneider (2006)

¹²Schneider (2006)

is given by the following equation:

$$\rho_{cr,0} = \frac{3H_0^2}{8\pi G}.^{13} \quad (2.4)$$

The critical density gives us an easy way to define the dimensionless cosmological density parameters, the parameters that describe the physical make-up of the contents of the universe. We can define the dimensionless baryon, dark matter, radiation and dark energy density parameters (defined at the present) as follows:

$$\Omega_b = \frac{\rho_b}{\rho_{cr,0}}, \Omega_c = \frac{\rho_c}{\rho_{cr,0}}, \Omega_\Lambda = \frac{\rho_\Lambda}{\rho_{cr,0}} = \frac{\Lambda}{3H_0^2}, \Omega_r = \frac{\rho_r}{\rho_{cr,0}}.^{14} \quad (2.5)$$

What these equations provide is an understanding of what exactly the density parameters mean and how they relate to physically real densities with proper units. Note that for the purpose of this thesis, Ω_r includes contributions of both photon and neutrino densities. It should also be noted that, the overall matter content of the universe can be defined to be the sum of baryonic matter and dark matter:

$$\Omega_m = \Omega_b + \Omega_c.^{15} \quad (2.6)$$

The cosmological density parameter, Ω_0 , is the overall density of the universe, and is given by the sum of the matter contents of Ω_m with the radiation density Ω_r and the vacuum energy density, Ω_Λ . This relation gives:

$$\Omega_0 = \Omega_m + \Omega_r + \Omega_\Lambda.^{16} \quad (2.7)$$

The cosmological density parameter is inherently related to the spatial curvature parameter k as follows:

$$k = \left(\frac{H_0^2}{c^2}\right)(\Omega_0 - 1).^{17} \quad (2.8)$$

This comes from Equation 2.1 substituting in our definitions for the dimensionless parameters. Note that the spatial curvature, k , has dimensions of $1/m^2$, and is not dimensionless like the other parameters. We can make k dimensionless, which is how many groups define the curvature parameter. This is done by the following definition:

$$\Omega_k = \Omega_0 - 1 = \frac{kc^2}{H_0^2}. \quad (2.9)$$

Some texts just use Ω_0 to refer to curvature, but sticking to the notation that CAMB uses, I will be using the above expression for the purposes of this paper.

The final point of theory which I will go over is the scaled Hubble constant, h . This parameter encodes the uncertainty associated with measurements of the Hubble

¹³Schneider (2006)

¹⁴Schneider (2006)

¹⁵Schneider (2006)

¹⁶Schneider (2006)

¹⁷Schneider (2006)

constant and scales it from a set value of $100 \text{ km s}^{-1} \text{ Mpc}^{-1}$ as defined.¹⁸ Thus the Hubble constant is given by the following relation:

$$H_0 = 100h \text{ km s}^{-1} \text{ Mpc}^{-1}.^{19}$$
 (2.10)

For the Planck value of the Hubble constant, we have $h \approx 0.7$, making the constant approximately $70 \text{ km s}^{-1} \text{ Mpc}^{-1}$.²⁰ We can encode this uncertainty into the density parameters to give what is known as the “physical” density parameters, which are given by: $\Omega_b h^2$, $\Omega_c h^2$, and so on for any density parameter.²¹ These are usually how the parameters are represented, but for the purposes of this paper, they will be represented as Ω_b and Ω_c .

2.1.1 Baryon Density, Ω_B

The baryon density is a very important and famous fraction in the field of cosmology. We have already seen, in Chapter 1, that this parameter is intimately related to the compression and rarefaction of the subsequent baryonic acoustic oscillations. Increasing the baryon content of the universe subsequently increases the effect of the aforementioned baryon drag which increases relative anisotropy contributions in the odd-numbered peaks of the power spectrum and lowers the relative contributions of even-numbered peaks.²² Alternatively, decreasing the baryon content will have the opposite effect. These effects are shown in Figure 2.2. As a result, the baryon density parameter is encoded in the heights of the peaks of the power spectrum.²³ One can also see in the figure that the peak multipole moments are also shifted slightly as the odd and even peaks occur at different locations. This multipole shifting is a byproduct of the wavelength of baryonic acoustic oscillations changing, which effectively changes the angular scale at which the peaks occur.

Looking at the dependent parameters, raising the baryon density decreases the dark energy density and increases the mass density as the curvature is kept constant, which makes sense given the curvature parameter’s proportionality to the overall density parameter Ω_0 . Changing this baryon density doesn’t change the radiation density, but interestingly the age of the universe decreases as baryon density increases. The age of the universe decreases with a raised baryon density because, if we make a plot of the scale factor of the universe, a vs. time, shown in Figure 2.1, increased matter density makes the plot more concave before branching off with a slope related to the Hubble constant. This increased concavity occurs because matter increases gravitation which opposes expansion and draws the universe closer together. Essentially, with increased concavity, comes a shorter time interval from $t=0$ (the Big Bang) to the present day t_0 .

¹⁸Schneider (2006)

¹⁹Schneider (2006)

²⁰Planck Collaboration, et al. (2020b)

²¹Schneider (2006)

²²Hu

²³Hu

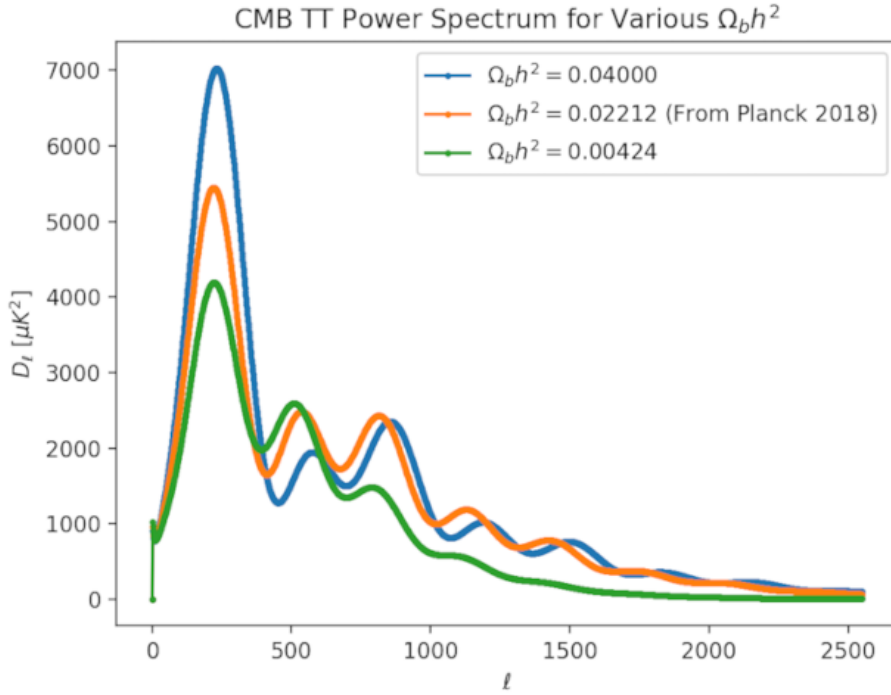


Table 2.3: Dependent parameters varying baryon density.

Ω_b	Ω_Λ	Ω_r	Ω_m	t_0 (Gyr)
0.00948	0.718	0.0015	0.279	14.350
0.04945 (P18)	0.678	0.0015	0.319	13.826
0.08943	0.638	0.0015	0.359	13.371

Figure 2.1: The temperature power spectrum of the CMB plotted using CAMB with various values of the baryon density parameter, Ω_b . The central value of Ω_b is the Planck 2018 value labeled by P18. The rest of independent parameters are given by the Planck 2018 values. The specific values shown for Ω_b were chosen such that they noticeably exemplify the behavior of the power spectrum for values above and below the Planck 2018 Ω_b . Also shown is a table that lists the dependent parameters for each baryon density.

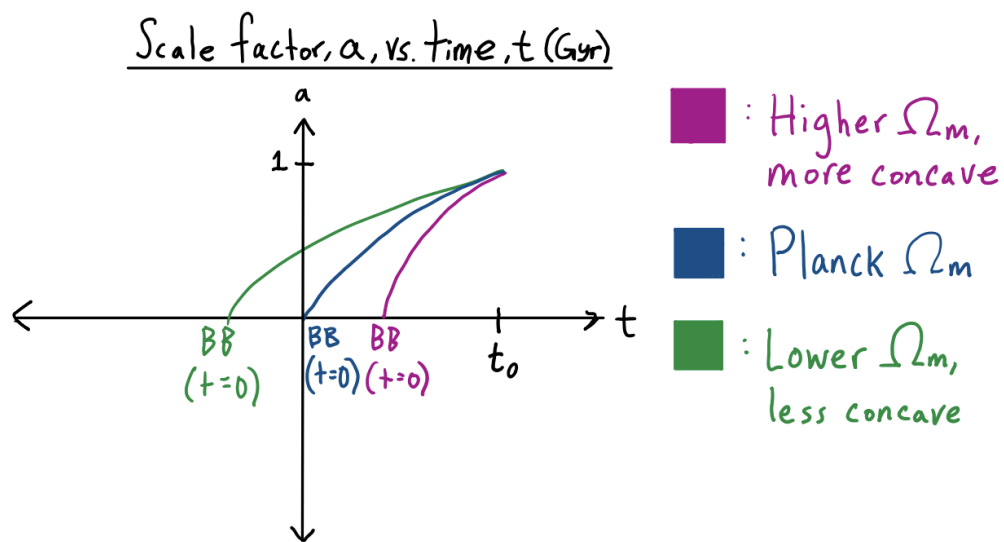


Figure 2.2: A sketch of the plot of the scale factor of the universe, a , vs. time, t , for raised and lowered values of Ω_m . Raised values of Ω_m make the graph more concave, decreasing the age of the universe (as seen on the time axis) whereas lowered values of Ω_m make the graph less concave, increasing the age of the universe.

2.1.2 Dark Matter Density, Ω_c

At the edges of galaxies, we have witnessed faster movement than anticipated, suggesting the gravitational influence of a type of matter that doesn't electromagnetically interact. This gravitational influence was first witnessed by Fritz Zwicky in 1933 in the Coma galaxy cluster, but has been witnessed in other galaxy rotations by Vera Rubin the 1970s. These gravitational influences have also been seen elsewhere and act as strong evidence for the existence of dark matter.²⁴ The effects of this matter, which is presumed to be non-relativistic (hence being dubbed "cold dark matter") can be seen and detected in the power spectrum of the CMB.²⁵ The dark matter content, along with the baryon content, add together to give the overall matter content of the universe, Ω_m . The effects of including dark matter in the Λ CDM model create an interesting dependence on the power spectrum of the CMB. These effects can be shown in Figure 2.3. As can be seen, the height of the first peak is decreased for an increasing dark matter density (from the Planck 2018 value), and subsequently higher peaks are reduced. This reduction in peak height occurs because an increased dark matter density reduces the effect of baryon drag given greater strength of dark matter potential wells.²⁶ For a decreased value of the dark matter density parameter, the opposite occurs where the first peak height is increased and the even ordered peaks increase relative to the odd peaks. The relative peak height shift occurs because decreasing the dark matter density decreases the strength of their gravitational wells, meaning that baryons then have nothing to fall into besides their own gravitational interactions.²⁷ This reasoning is also why with baryons, the height of the first peak is decreased for an decreased baryon content, whereas with dark matter, the first peak is increased with an decreasing density, as the lack of potential wells increases anisotropy in first few modes. Subsequently, the peak heights alter according to the ratio of baryons to dark matter.

Increasing the dark matter density parameter subsequently decreases the dark energy density for the same reason that increasing baryon density decreases dark energy for a constant curvature parameter that is proportional to the sum of matter, radiation and dark energy. The dark energy density is more sensitive to the dark matter density given that there is a significantly larger amount of dark matter in the universe. Further, just as the baryon density, the dark matter density does not impact the radiation density. The dark matter density drastically decreases the age of the universe relative to the baryon density, which is also due to the fact that the dark matter density is larger overall. The age of the universe decreases for an increasing dark matter density for the same reason that the age of the universe decreases for increasing the baryon density, as subsequently both contribute to the matter density Ω_m . If the matter density Ω_m is greater, the plot of the scale factor vs. time is more concave, decreasing the age of the universe, as shown by Figure 2.1.

²⁴Schneider (2006)

²⁵Schneider (2006)

²⁶Hu

²⁷Hu

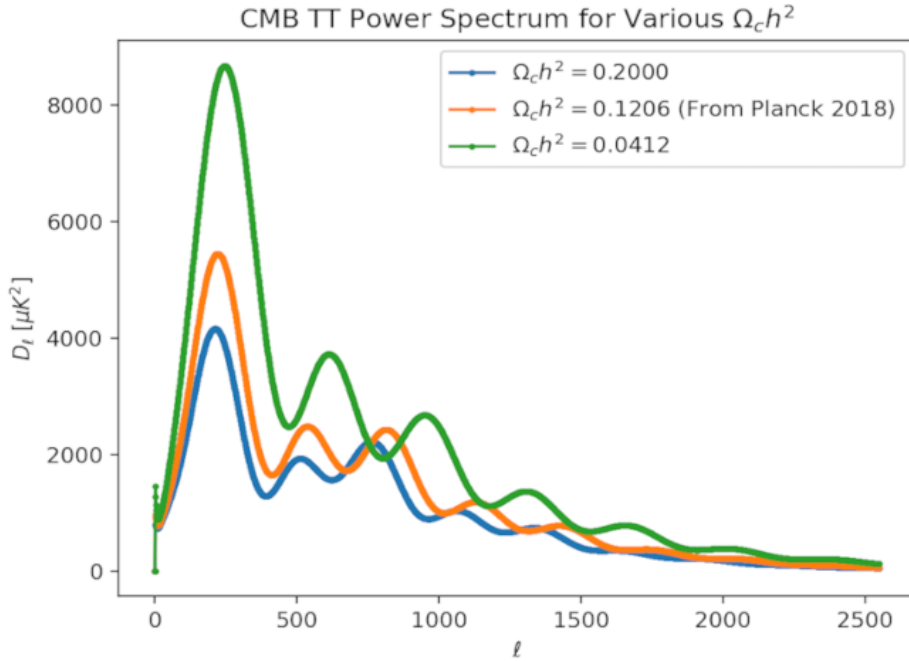


Table 2.4: Dependent parameters varying dark matter density.

Ω_c	Ω_Λ	Ω_r	Ω_m	t_0 (Gyr)
0.0921	0.856	0.0015	0.142	17.114
0.2696 (P18)	0.678	0.0015	0.319	13.826
0.4471	0.501	0.0015	0.497	12.158

Figure 2.3: A figure showing the temperature power spectrum of the CMB plotted using CAMB with various values of the dark matter density parameter, Ω_c . The rest of the parameters are given by the Planck 2018 values. The specific values shown for Ω_c were chosen such that they noticeably exemplify the behavior of the power spectrum for values above and below the Planck 2018 Ω_c . Also shown is a table that lists the dependent parameters for each dark matter density, keeping the other 5 base parameters constant.

2.2 Summed Neutrino Mass, m_ν

The added mass of every type of neutrino is given by the parameter m_ν , and is typically denoted in units of eV. This parameter is chosen to be represented as a mass rather than a dimensionless density because it is useful to represent as such for the calculation of dependent parameters. Nevertheless, it is obviously intimately related to the neutrino mass density, Ω_ν . About a second after the Big Bang, neutrinos also decoupled from matter, creating what is known as the cosmic neutrino back-

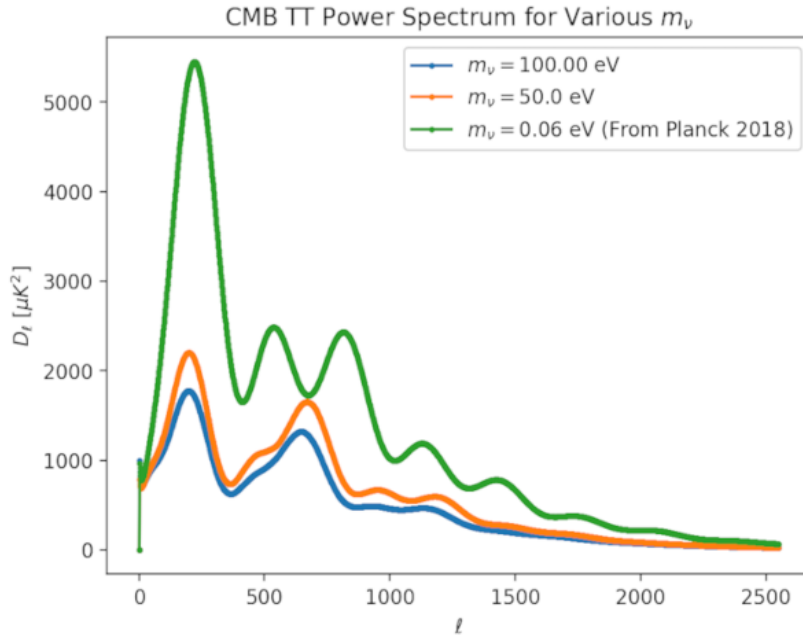


Table 2.5: Dependent parameters varying the summed neutrino mass.

m_ν (eV)	Ω_Λ	Ω_r	Ω_m	t_0 (Gyr)
0.06 (P18)	0.678	0.0015	0.319	13.826
50.00	-0.522	1.2015	0.319	8.442
100.00	-1.723	2.4029	0.319	6.823

Figure 2.4: A plot showing the temperature power spectrum of the CMB plotted using CAMB with various values of the summed neutrino mass parameter, m_ν . The rest of the parameters are given by the Planck 2018 values. The specific values shown for m_ν were chosen such that they noticeably exemplify the behavior of the power spectrum for values above Planck 2018 m_ν , since lower values are harder to distinguish between and produce approximately the same spectrum as $m_\nu = 0.06 \text{ eV}$. Also shown is a table that lists the dependent parameters for each summed neutrino mass, keeping the other 5 base parameters constant.

ground (CNB).²⁸ The CNB is extremely hard to measure given that neutrinos do not interact electromagnetically and are close to massless. Luckily, the CMB power spectrum is very dependent on the sum of the neutrino masses above 0.06eV. This dependency occurs because changing the neutrino mass changes the time of matter-radiation equality, and influences expansion and curvature as a component of Ω_r .²⁹ What results is that the value of m_ν distorts the power spectrum structure. This

²⁸Schneider (2006)

²⁹Abazajian, K N, et al. (2013)

power spectrum distortion is shown in Figure 2.4. A related parameter is the effective number of neutrino species, which is predicted by the CMB to be approximately 3.³⁰

One can see that if neutrinos are sufficiently massive, the anisotropy of the CMB is significantly reduced and distorted. The distortion seems to eliminate the 2nd peak as it combines with the third. The trend seems to indicate that as the mass of neutrinos is increased, the peak heights and distances from each other will be reduced to the point where only the first and third peaks will remain distinguishable. As the neutrino mass gets smaller, the power spectrum distorts less and less, and it becomes harder to distinguish between its value. The Planck 2018 group has constrained the sum neutrino mass to be less than or equal to 0.06 eV.³¹ Choosing $m_\nu = 0.06$ eV fits with the Planck 2018 power spectrum, so this value is what is typically chosen when constructing the CAMB spectrum.

Changing the summed neutrino mass, as I have done in this experiment, drastically impacts the dependent parameters, quickly making it clear which value is most consistent with our universe. If the summed neutrino mass is increased the dark energy density decreases drastically becoming negative and larger than 1 in magnitude. The opposite occurs for the radiation density as it increases and becomes closer to 2 in magnitude. Subsequently, the mass density is not impacted by increasing the neutrino mass, but the age of the universe drastically decreases.

2.3 Hubble Constant, H_0

In 1929 a paper was released by Edwin Hubble with data suggesting that galaxies are apparently moving away from us at a rate known now as the Hubble constant.³² Several other astronomers such as Henrietta Leavitt contributed greatly to this discovery as well. The Hubble Law can be expressed as follows:

$$v = H_0 D, \quad (2.11)$$

where v represents the radial velocity of galaxies and D represents their distance.³³ The Hubble constant is a cosmological parameter that is of great importance to the Λ CDM model. Its precise value is famously contested, as different techniques (including measurement using the CMB temperature power spectrum) can provide different values. It is currently estimated to be around $66.88 \text{ km s}^{-1} \text{ Mpc}^{-1}$.³⁴ The power spectrum responds to changes in the Hubble constant as shown in Figure 2.5.

This figure shows that decreasing the Hubble constant corresponds to a stretching of the power spectrum along the x-direction. This power spectrum stretching has the greatest impact towards multipoles of $\ell = 1000 - 1500$ multipoles. There may also be a slight translational effect, but it is hard to distinguish and much less pronounced

³⁰Abazajian, K N, et al. (2013)

³¹Planck Collaboration, et al. (2020b)

³²Hubble (1929)

³³Schneider (2006)

³⁴Planck Collaboration, et al. (2020b)

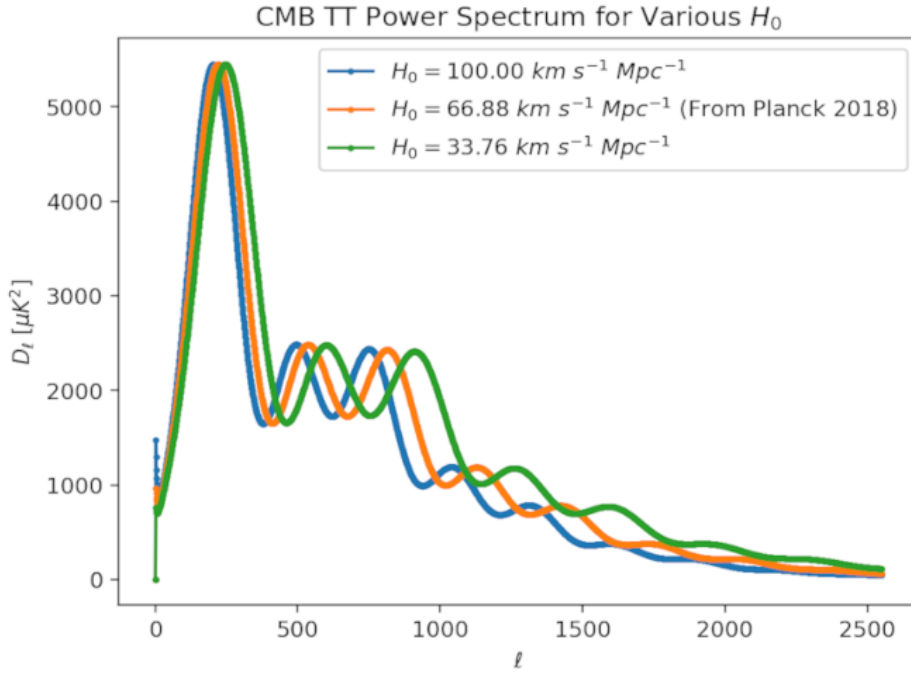


Table 2.6: Dependent parameters varying the Hubble constant.

$H_0 (\text{km s}^{-1} \text{ Mpc}^{-1})$	Ω_Λ	Ω_r	Ω_m	$t_0 (\text{Gyr})$
33.76	-0.259	0.0057	1.252	17.858
66.88 (P18)	0.678	0.0015	0.319	13.826
100.00	0.856	0.0007	0.143	11.444

Figure 2.5: A plot of the temperature power spectrum of the CMB plotted using CAMB with various values of the Hubble constant, H_0 . The rest of the parameters are given by the Planck 2018 values. The specific values shown for H_0 were chosen such that they noticeably exemplify the behavior of the power spectrum for values above and below the Planck 2018 H_0 . Also shown is a table that lists the dependent parameters for each value of the Hubble constant, keeping the other 5 base parameters constant.

than that of the curvature parameter.

Increasing the Hubble constant has a great effect on all of the chosen density parameters. The dark energy density drastically increases as the Hubble constant decreases, and if the Hubble constant is too small, it becomes negative corresponding to a universe that is contracting, which doesn't fit Hubble's observations. Meanwhile, the radiation density decreases drastically, as does the matter density from a value close to 1. The age of the universe subsequently also decreases as the universe expands faster to the present day.

2.4 Curvature Parameter, Ω_k

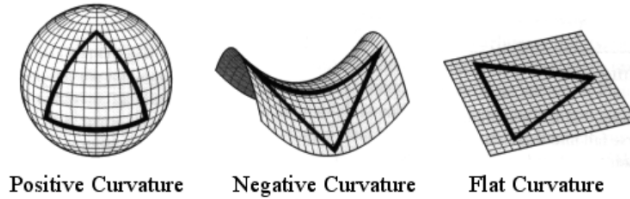


Figure 2.6: The three spatial curvatures of a homogeneous and isotropic universe. The “positive” geometry corresponds to positive Ω_k , the “negative” geometry corresponds to negative Ω_k , and the flat geometry corresponds to $\Omega_k = 0$. *Image Credit: Schneider (2006)*

There are three shapes of the universe that are consistent with both homogeneity and isotropy, as required by Einstein’s cosmological principle. These are geometries are labeled by the sign of Ω_k they correspond to. The “positive curvature” geometry has a positive curvature parameter and corresponds to the 2D analogy of a the surface of a sphere. The “negative curvature” geometry describes a negative curvature parameter and can be represented by the 2D analogy of a hyperboloid much like the surface of a saddle. Finally, the flat configuration is given by a curvature parameter of zero and is analogous to flat sheet.³⁵ These 3 shapes are shown in Figure 2.6. One can see from the CAMB plot in Figure 2.7 that the exact peak location is dependent on the curvature parameter, where an increasingly negative parameter shifts the plot to the left, and an increasingly positive parameter shifts the plot to the right. Through these translations the structure of the peak heights and shape remain relatively the same. This peak height invariance occurs because the curvature defines exactly how angular scale changes, but doesn’t alter the intensity of anisotropy from the relative contributing multipole.

Increasing the curvature parameter decreases the dark energy density, but the radiation and matter densities stay the same. This matter density invariance is a result of keeping the baryon density and the dark matter density constant for this experiment. Further, the age of the universe decreases, which is surprising given the decrease in the dark energy density. Nonetheless, one can see how the curvature of the universe expands and contracts the age of the universe.

³⁵Schneider (2006)

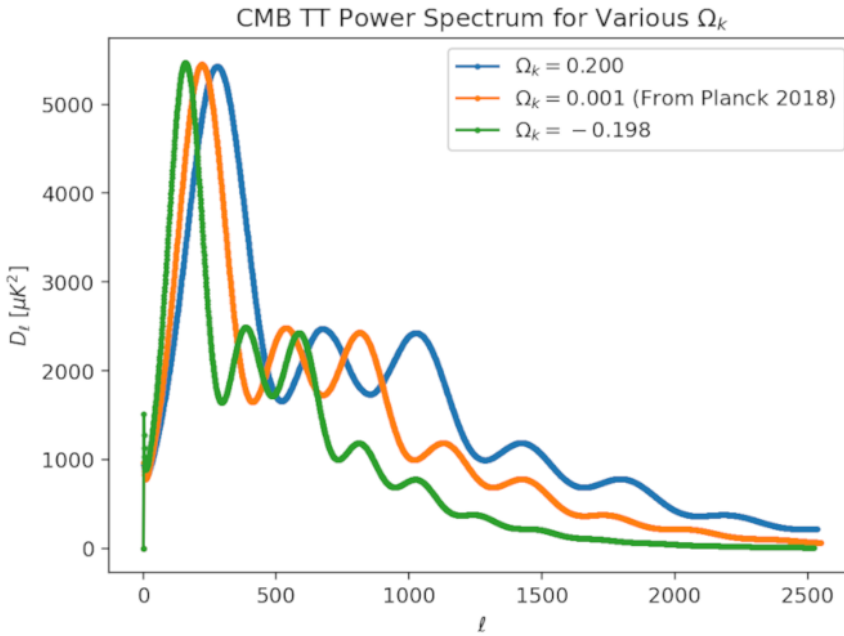


Table 2.7: Dependent parameters varying the curvature parameter.

Ω_k	Ω_Λ	Ω_r	Ω_m	t_0 (Gyr)
-0.198	0.877	0.0015	0.319	14.768
0.001 (P18)	0.678	0.0015	0.319	13.826
0.200	0.479	0.0015	0.319	13.072

Figure 2.7: The temperature power spectrum of the CMB plotted using CAMB with various values of the curvature parameter, Ω_k . The rest of the parameters are given by the Planck 2018 values. The specific values shown for Ω_k were chosen such that they noticeably exemplify the behavior of the power spectrum for values above and below the Planck 2018 Ω_k . Also shown is a table that lists the dependent parameters for each curvature parameter, keeping the other 5 base parameters constant.

2.5 Reionization Optical Depth, τ

Prior to recombination, the universe was ionized given that electrons hadn't yet joined with atomic nuclei. After recombination the universe entered the "dark ages" where atoms as we know it with electron orbitals formed, making the universe itself transparent because of the longer mean free path of light.³⁶ Much after recombination and until the present day (occurring in a range of redshifts from 0 to roughly 6), the

³⁶Maoz (2016)

universe became reionized as the first stars and galaxies formed.³⁷ This process is not very well understood, but it is an important moment in the history of large-scale structure formation of the universe as early stars began to shine.

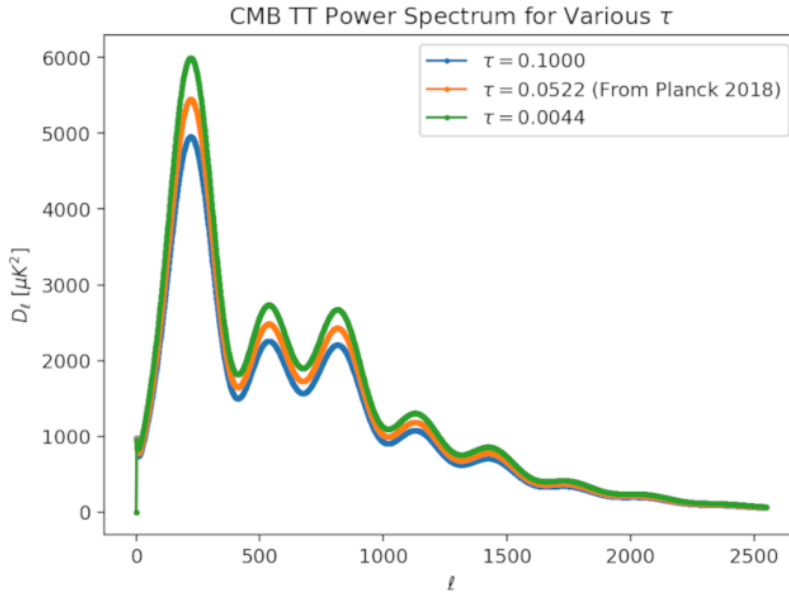


Table 2.8: Dependent parameters varying the reionization optical depth.

τ	Ω_Λ	Ω_r	Ω_m	t_0 (Gyr)
0.0044	0.678	0.0015	0.319	13.826
0.0522 (P18)	0.678	0.0015	0.319	13.826
0.1000	0.678	0.0015	0.319	13.826

Figure 2.8: The temperature power spectrum of the CMB plotted using CAMB with various values of the reionization optical depth, τ . The rest of the parameters are given by the Planck 2018 values. The specific values shown for τ were chosen such that they noticeably exemplify the behavior of the power spectrum for values above and below the Planck 2018 τ . Also shown is a table that lists the dependent parameters for each reionization optical depth, keeping the other 5 base parameters constant.

When the universe became reionized, a large scale obstruction to the movement of CMB photons occurred because of Thompson scattering, where photons are deflected by slower moving ions.³⁸ The way in which this obstruction is parameterized is by an optical depth, τ , which is related to the fraction of transmitted vs. incident photon intensities. Ultimately this leads to a characterization of the optical depth that is

³⁷Maoz (2016); Barkana & Loeb

³⁸Schneider (2006)

dependent on the mass and baryon densities given that these quantities alter when reionization occurs.³⁹ The reionization optical depth is characterized as such:

$$\tau = 0.041 \frac{\Omega_b h}{\Omega_m} ((1 - \Omega_m + \Omega_m(1 + z_{\text{re}})^3)^{1/2} - 1).^{40} \quad (2.12)$$

In this equation, z_{re} represents the redshift at which reionization occurs. Unsurprisingly, the CMB power spectrum is altered by Thompson scattering of CMB photons, and thus effected by changes in τ .⁴¹ Interestingly, τ is a very important parameter because the other parameters are not dependent on it.⁴² This lack of dependence makes it essential for the Λ *CDM* model to characterize reionization. Figure 2.8 shows the dependence of the CMB power spectrum on the reionization optical depth. As can be seen, for increasing values of τ , the height of the entire curve is lowered. This means the precise peak height of the entire curve is dependent on τ . This effect occurs because greater Thompson scattering blends photons from seemingly different lines of sight and reduces the clarity of primordial CMB fluctuations.⁴³

If we look at the dependent parameters, as expected none of them change with an increasing reionization optical depth. This highlights the importance of this parameter given that it adds the effect of reionization into the model, and given that not many other parameters are dependent on its value besides the reionization redshift.

2.6 Consistency with Planck Parameters

Figure 2.9 shows my data in comparison with the CAMB plot inputting the six parameters using Planck 2018 values, shown in Table 2.9. As one can see from the plot, my data are in close alignment with the CAMB-produced plot. The CAMB plot seems to be mostly within the error bars determined by considering cosmic variance, with some areas where the values seem slightly larger than the Planck graph, likely due to noise/not fully including error from sources other than cosmic variance. This correspondence indicates that the Planck values of the base 6 cosmological parameters are consistent with the power spectra generated for this thesis. Hence, the methods of parameter extraction used in this paper prove to be relatively accurate given our current best estimates. These parameters describe a close to flat universe, with notable contributions of dark energy and dark matter, all of which correspond well to the Λ *CDM* model.

³⁹Barkana & Loeb

⁴⁰Barkana & Loeb

⁴¹Planck Collaboration, et al. (2020b)

⁴²Schneider (2006)

⁴³Barkana & Loeb

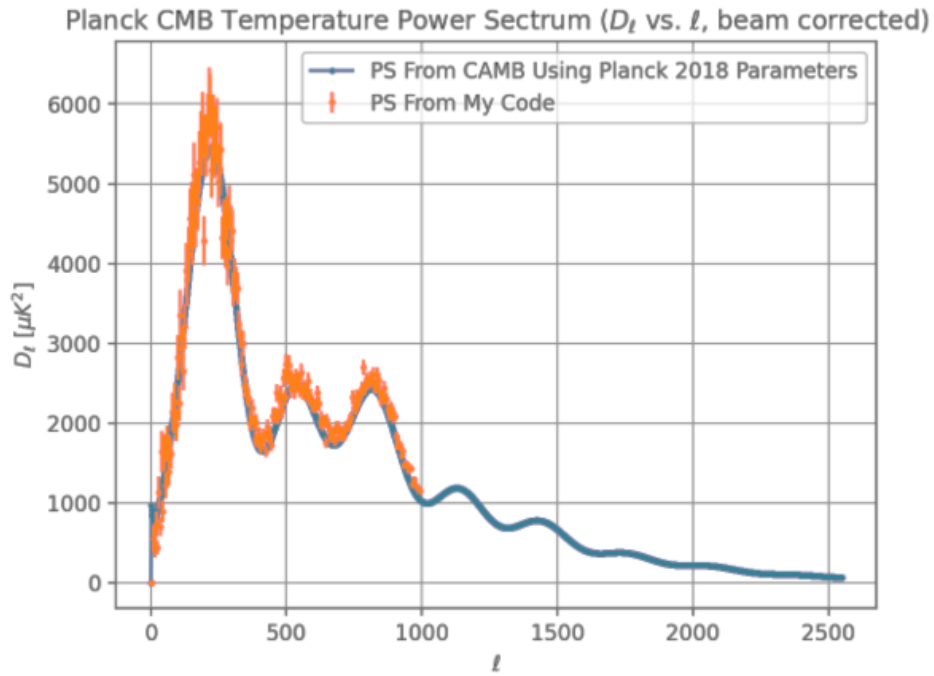


Table 2.9: Planck 2018 Parameter Values

Parameter	Value
H_0	$66.88 (\pm 0.92) \text{ km s}^{-1} \text{ Mpc}^{-1}$
Ω_b	$0.04945 (\pm 0.00002)$
Ω_c	$0.2696 (\pm 0.0047)$
m_ν	$\leq 0.06 \text{ eV}$
Ω_k	$0.001 (\pm 0.002)$
τ	$0.0522 (\pm 0.0080)$

Figure 2.9: The temperature power spectrum of the CMB plotted with the methods used in this paper and using CAMB with Planck 2018 parameters. Also shown is a table listing the values of the base 6 parameters found by the Planck Collaboration.

Chapter 3

CosmoMC and Extensions

The method of cosmological parameter estimation using the cosmic microwave background temperature maps proves to be a great way to re-derive the results of the Planck collaboration. Though this research is not novel in the sense that many physicists have produced the very same results, detailing this process has given me an understanding of the rich physics of the cosmic microwave background, a topic anyone interested in cosmology should study. All the different contributions to anisotropy are ripe with effects that span a wide range of topics in the study of physics. Further, the study itself gives key insights into the universe under the constraints of the Λ CDM model, which currently stands as the standard model of cosmology with the most accurate predictions as of the present day.

Ultimately the extraction of parameters in this paper is relatively imprecise and they don't have easily calculable errors which is highly important to the field of cosmology. In order to get more precise cosmological parameter estimates with errors, a package related to CAMB called CosmoMC must be used. Essentially, CosmoMC performs a Markov Chain Monte-Carlo analysis on input power spectra. Essentially, Markov Chain Monte-Carlo involves sequencing random samples to create a Markov chain of randomized parameters that approximates an input distribution.¹ Within the Markov chain are the parameters that produce the proper distribution matching the input distribution, allowing for calculation of errors using parameter values that are close by.² In this case CosmoMC calls CAMB over and over again randomizing parameter values to find a chain that fits input power spectra. These parameter chains that can then be sent to an associated package called `getDist`, which can subsequently extract the parameters and their errors. This method of using CosmoMC and `getDist` is exactly how the Planck 2018 group produced their very precise parameter estimates with errors.³ `getDist` can also be used to explore parameter space, and how various cosmological parameters change with respect to each other. The Planck Collaboration produced parameter chains from CosmoMC, which can be found in their 2018 data release, using the power spectra they produced. A few plots using this `getDist` code are shown in Figure 3.1. These figures show how the parameter values and likelihoods

¹Speagle (2020)

²Speagle (2020)

³Planck Collaboration, et al. (2014)

change with respect to each other for a few different parameters. This allows us to explore the 6-dimensional parameter space of Λ CDM using Planck data, both with independent and dependent parameters.

Unfortunately, using CosmoMC to get more accurate parameters with errors is out of the scope of this thesis due to time constraints, as I chose to focus on power spectrum generation and optimization to get to the parameters, but utilizing CosmoMC on the power spectra produced by the methods of this thesis would be a great extension of this project. In order to get CosmoMC to run, Linux is required as an operating system. Once this requirement is satisfied, the program itself can be downloaded and power spectra can be uploaded to obtain parameter chains. `getDist` can then extract parameter values with proper errors from these parameter chains, as I have done with the Planck 2018 parameter chains.

In the modern era of cosmology, determining these parameters to better precision is a big goal given that there are discrepancies in values of certain parameters, based on different methods of estimation. A few of these discrepancies, to name are the missing baryon problem, and the Hubble tension which describe discrepancies in values of the baryon density and the Hubble constant. The Hubble tension specifically comes from measurements of Hubble's constant using the distance of galactic bodies detected by telescopes (such as the Hubble telescope and the James Webb telescope), which doesn't align with the Planck satellite's measurements.⁴ Either this is an indication of new physics beyond the Λ CDM model, or an inherent error with either measurement process.⁵ The missing baryon problem comes from the fact that observed baryon density due to a number of contributions is less than that of the baryon density calculated from the cosmic microwave background by as much as 7% of the cosmic value.⁶ It is believed that these baryons likely reside in the intergalactic medium, but still disagrees with the value from the CMB.⁷ Surely, solving these discrepancies will reveal new secrets about the universe, its origins, and ultimately its fate. The main way to really peer into these discrepancies is through a deep review of the techniques by which we determine these parameters. The goal of this thesis is to provide insight into one particular method of determining cosmological parameters, to be used as a resource for those who wish to replicate the same analyses for deeper studies. Hopefully, one day, these issues in cosmology will be solved, as we revise our models to better encapsulate the universe on the largest scales.

⁴Hu & Wang (2023)

⁵Hu & Wang (2023)

⁶Yang et al. (2022)

⁷Yang et al. (2022)

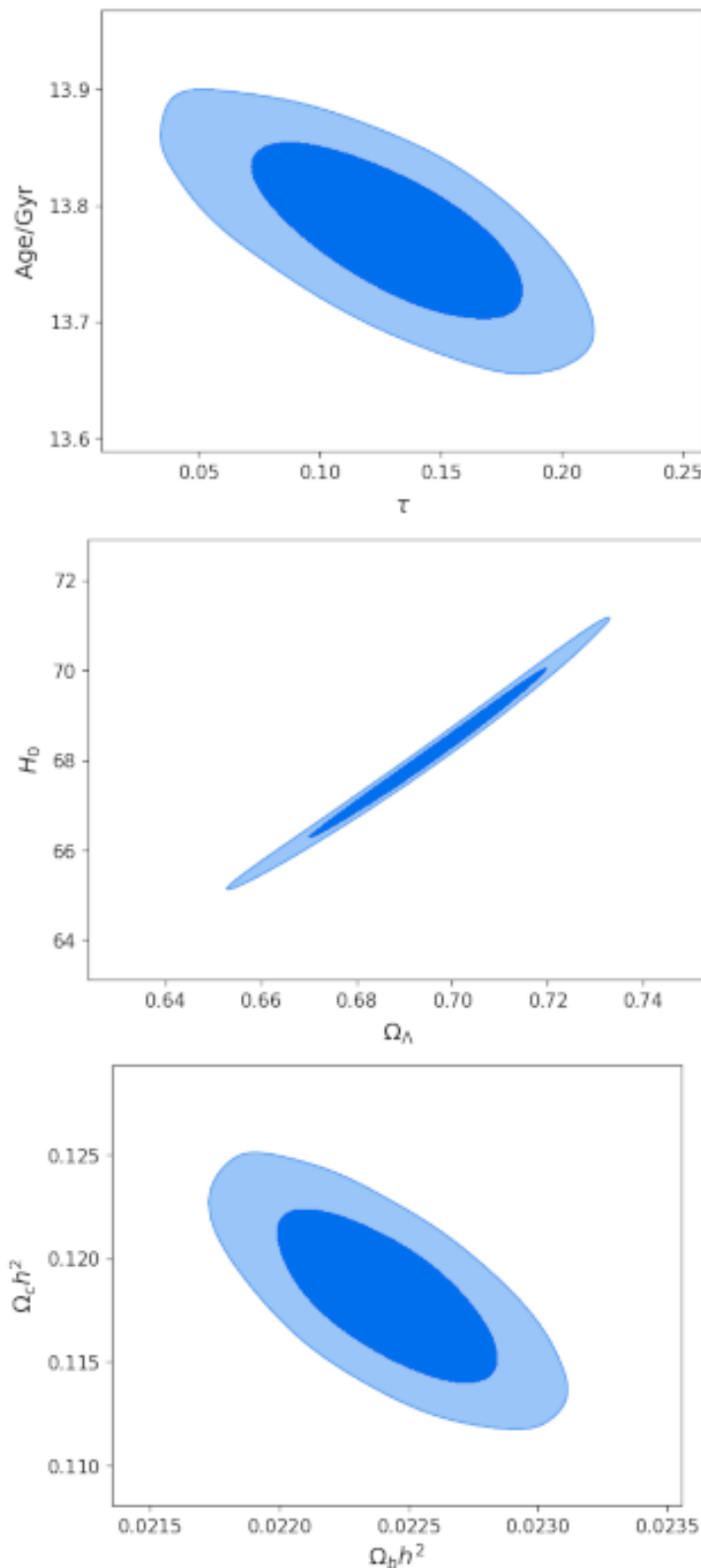


Figure 3.1: A figure showing getDist plots using Planck 2018 parameter chains. These plots show how various parameters and their likelihoods change with respect to each other. The plots shown are t_0 vs. τ , H_0 vs. Ω_Λ , and $\Omega_c h^2$ vs. $\Omega_b h^2$. Light blue regions indicate 68% confidence in the value while dark blue regions indicate 95% confidence.

References

- (n.d.). Centre for Theoretical Cosmology: The Origins of the Universe: Inflation Introduction. https://www.ctc.cam.ac.uk/outreach/origins/inflation_zero.php
- Abazajian, K N, et al. (2013). Neutrino Physics from the Cosmic Microwave Background and Large Scale Structure.
- Ade, P. a. R., et al. (2014). Planck 2013 results. VII. HFI time response and beams. *Astronomy & Astrophysics*, 571, A7. Publisher: EDP Sciences. <https://www.aanda.org/articles/aa/abs/2014/11/aa21535-13/aa21535-13.html>
- Barkana, R., & Loeb, A. (n.d.). Reionization Review - R. Barkana & A. Loeb. <https://ned.ipac.caltech.edu/level5/March01/Barcana/Bar9.html>
- Bennett, C. L., et al. (2013). Nine-Year Wilkinson Microwave Anisotropy Probe (WMAP) Observations: Final Maps and Results. *The Astrophysical Journal Supplement Series*, 208(2), 20. ArXiv:1212.5225 [astro-ph]. <http://arxiv.org/abs/1212.5225>
- Birkinshaw, M. (n.d.). The Sunyaev-Zel'dovich Effect. https://ned.ipac.caltech.edu/level5/Birkinshaw/Birk11_3.html
- Cabass, Giovanni, et al. (2015). Constraints on the Early and Late Integrated Sachs-Wolfe effects from Planck 2015 Cosmic Microwave Background Anisotropies angular power spectra. *Physical Review D*, 92(6), 063534. ArXiv:1507.07586 [astro-ph, physics:hep-ph]. <http://arxiv.org/abs/1507.07586>
- Callin, P. (2006). How to calculate the CMB spectrum. ArXiv:astro-ph/0606683. <http://arxiv.org/abs/astro-ph/0606683>
- Carroll, B., & Ostlie, D. (2014). *An Introduction to Modern Astrophysics*. Pearson custom library. Pearson. <https://books.google.com/books?id=RLwangEACAAJ>
- Dicke, R. H., et al. (1965). Cosmic Black-Body Radiation. *The Astrophysical Journal*, 142, 414–419. ADS Bibcode: 1965ApJ...142..414D. <https://ui.adsabs.harvard.edu/abs/1965ApJ...142..414D>

- Gerbino, Martina, et al. (2020). Likelihood Methods for CMB Experiments. *Frontiers in Physics*, 8. <https://www.frontiersin.org/articles/10.3389/fphy.2020.00015>
- Gorski, Krzysztof M., et al. (1999). The HEALPix Primer. ArXiv:astro-ph/9905275. <http://arxiv.org/abs/astro-ph/9905275>
- Hu, J.-P., & Wang, F.-Y. (2023). Hubble Tension: The Evidence of New Physics. ArXiv:2302.05709 [astro-ph, physics:hep-th]. <http://arxiv.org/abs/2302.05709>
- Hu, W. (n.d.). Wayne Hu's Tutorials. <http://background.uchicago.edu/>
- Hubble, E. (1929). A Relation between Distance and Radial Velocity among Extra-Galactic Nebulae. *Proceedings of the National Academy of Science*, 15, 168–173. ADS Bibcode: 1929PNAS...15..168H. <https://ui.adsabs.harvard.edu/abs/1929PNAS...15..168H>
- Jungman, G., et al. (1996). Cosmological-Parameter Determination with Microwave Background Maps. *Physical Review D*, 54(2), 1332–1344. ArXiv:astro-ph/9512139. <http://arxiv.org/abs/astro-ph/9512139>
- Maoz, D. (2016). *Astrophysics in a Nutshell: Second Edition*. Princeton University Press. Google-Books-ID: 9GuYDwAAQBAJ.
- Mather, e. a., J. C. (1990). A Preliminary Measurement of the Cosmic Microwave Background Spectrum by the Cosmic Background Explorer (COBE) Satellite. *The Astrophysical Journal*, 354, L37. ADS Bibcode: 1990ApJ...354L..37M. <https://ui.adsabs.harvard.edu/abs/1990ApJ...354L..37M>
- Mo, Houjun., et al. (2010). *Galaxy formation and evolution*. Cambridge ;: Cambridge University Press. Publication Title: Galaxy formation and evolution.
- Peebles, P. J. E. (1993). *Principles of Physical Cosmology*. Publication Title: Principles of physical cosmology ADS Bibcode: 1993ppc..book.....P. <https://ui.adsabs.harvard.edu/abs/1993ppc..book.....P>
- Penzias, A. A., & Wilson, R. W. (1965). A Measurement of Excess Antenna Temperature at 4080 Mc/s. *The Astrophysical Journal*, 142, 419–421. ADS Bibcode: 1965ApJ...142..419P. <https://ui.adsabs.harvard.edu/abs/1965ApJ...142..419P>
- Planck Collaboration, et al. (2014). Planck 2013 results. XVI. Cosmological parameters. *Astronomy & Astrophysics*, 571, A16. ArXiv:1303.5076 [astro-ph]. <http://arxiv.org/abs/1303.5076>
- Planck Collaboration, et al. (2020a). Planck 2018 results. IV. Diffuse component separation. *Astronomy & Astrophysics*, 641, A4. ArXiv:1807.06208 [astro-ph]. <http://arxiv.org/abs/1807.06208>

- Planck Collaboration, et al. (2020b). Planck 2018 results. VI. Cosmological parameters. *Astronomy & Astrophysics*, 641, A6. ArXiv:1807.06209 [astro-ph]. <http://arxiv.org/abs/1807.06209>
- Schneider, P. (2006). *Extragalactic Astronomy and Cosmology: An Introduction*. Springer. <https://books.google.com/books?id=uP1Hz-6sHaMC>
- Speagle, J. S. (2020). A Conceptual Introduction to Markov Chain Monte Carlo Methods. ArXiv:1909.12313 [astro-ph, physics:physics, stat]. <http://arxiv.org/abs/1909.12313>
- Tegmark, M. (1995). Doppler peaks and all that: CMB anisotropies and what they can tell us. ArXiv:astro-ph/9511148. <http://arxiv.org/abs/astro-ph/9511148>
- Wright, E. L. (n.d.). Sachs-Wolfe Effect. <https://astro.ucla.edu/~wright/Sachs-Wolfe.html>
- Yang, K. B., Wu, Q., & Wang, F. Y. (2022). Finding the Missing Baryons in the Inter-galactic Medium with Localized Fast Radio Bursts. *The Astrophysical Journal Letters*, 940(2), L29. <https://iopscience.iop.org/article/10.3847/2041-8213/aca145>
- Zonca, A. (2020). Andrea Zonca - Read and process Planck CMB power spectra with healpy. <https://www.zonca.dev/posts/2020-09-30-planck-spectra-healpy.html>